J Mater Sci (2015) 50:2643–2665
DOI 10.1007/s10853-015-8855-x

REVIEW

On the correlation between microstructural evolution and ultrasonic properties: a review

Meysam Toozandehjani · Khamirul Amin Matori · Farhad Ostovan · Faizal Mustapha · Nur Ismarrubie Zahari · Arshin Oskoueian

Received: 27 August 2014 / Accepted: 12 January 2015 / Published online: 27 January 2015

Abstract The characterization and optimization of the microstructures of materials pertaining to material properties is a primitive necessity to ensure the performance and service life of the materials and components. In the demand of new characterization and evaluation techniques, nondestructive ultrasonic techniques have shown a good potential to characterize the microstructures and mechanical properties of a wide variety of materials. Measurements of ultrasonic parameters such as velocity and attenuation can provide information on the structural and microstructural variations of those materials that have undergone the heat-treatment procedure. In the current review, the correlation of ultrasonic parameters with microstructural features of ferrous and nonferrous metals such as steels, aluminum, and superalloys is investigated. It is proven that ultrasonic parameters are closely correlated to the microstructural evolutions which frequently occur during the heat-treatment procedures in practical situations. To conclude, the ultrasonic measurements contribute to a feasible and accurate characterization of the materials and evaluation of their microstructures and mechanical properties in a straightforward, reliable, and fast, nondestructive manner for practical applications.

M. Toozandehjani · K. A. Matori (✉) · F. Ostovan · A. Oskoueian
Materials Synthesis and Characterization Laboratory, Institute of Advanced Technology, Universiti Putra Malaysia, 43400 UPM Serdang, Selangor, Darul Ehsan, Malaysia
e-mail: khamirul@upm.edu.my

M. Toozandehjani
e-mail: Toozandejani.meysam@yahoo.com

F. Ostovan
e-mail: F.ostovan@gmail.com

A. Oskoueian
e-mail: arshin.oskoueian@gmail.com

F. Mustapha
Department of Aerospace Engineering, Faculty of Engineering, Universiti Putra Malaysia, 43400 Serdang, Selangor, Darul Ehsan, Malaysia
e-mail: faizalms@upm.edu.my

N. I. Zahari
Department of Mechanical Engineering, Faculty of Engineering, Universiti Putra Malaysia, 43400 Serdang, Selangor, Darul Ehsan, Malaysia
e-mail: rubie@upm.edu.my

Introduction

Manufacturing industries assign great efforts in obtaining a product with desired mechanical properties. Heat-treatment procedures are considered to be an effective tool to improve the mechanical properties of products in the manufacturing industries. The heat-treatment procedures are accompanied by variation in the microstructure which contributes, if correct procedure is followed, to achieving the desired mechanical properties of material [1–5].

The characterization of the material microstructures and corresponding mechanical properties are important in order to ensure the performance and service life of the components [1–3]. Techniques of material characterization are classified as destructive testing (DT) and nondestructive testing or evaluation (NDT or E). NDTs are introduced first as a substitute for destructive testings to confirm the functioning and the structural integrity of components and engineering products. NDTs are commonly employed for the purpose of detection and characterization of a variety of hidden flaws with respect to location, size, orientation, shape, and nature (if the flaw exists) [6–8]. NDE techniques have also shown potentials to evaluate the

microstructural features and mechanical properties of materials without making any damage and destruction. NDT and E techniques offer several advantages over the conventional destructive coupon-based techniques. These techniques are easy and fast to perform and can be directly applied during manufacturing as well as on actual components. 100 % coverage of component testing is possible. The information about the bulk material properties can be obtained owing to their volumetric nature. They can be considered as a potential, alternative analytic technique in the field of optical methods which demand sophisticated and time-consuming sampling and preparation [8–13].

Various nondestructive techniques have been currently employed to characterize the microstructural variations and mechanical properties of materials induced by heat-treatment procedures or high-temperature service condition. Each technique has its own advantages and disadvantages, and the choice of the technique relies on the desired approach. The common techniques are magnetic and electromagnetic techniques including eddy current testing (ECT) [9, 14–18], magnetic barkhaussen noise (MBN) [3, 13, 19–22], optical nondestructive techniques such as infrared thermography imaging and terahertz technology [23], as well as ultrasonic wave-based techniques. Among all available NDEs, ultrasonic techniques are considered as the most feasible technique for evaluation of microstructural and mechanical properties of materials.

Ultrasonic nondestructive technique, for characterization and evaluation purposes, has gained much interest during recent years. Many of researchers are engaged in characterizing different materials under various heat-treatment conditions by ultrasonic testing. Therefore, we start with giving a brief outline of the fundamentals of ultrasonic waves with emphasis on velocity and attenuation for better understanding, and then provide a review of researches conducted in the field of ultrasonic characterization of the various materials. The main purpose of this review paper is to investigate the correlation existing between microstructural variations underlying the heat-treatment processes and the ultrasonic parameters in a selection of alloys. Finally, the conclusions of the review have been pointed out.

Fundamental of ultrasonic testing and evaluation

The principle behind the ultrasonic testing is based on the fact that solid materials are good conductors of sound waves. Ultrasonic or ultrasound waves as a subcategory of acoustic waves possess all the characteristics of a sound wave. In fact, ultrasonic waves are defined as any acoustic wave with frequencies higher than 20 kHz which is above the threshold of human hearing range. Normally, ultrasonic techniques use high-frequency sound waves in the range of 0.5–10 MHz which propagate into materials to detect interior potential flaws or to find the characteristics of materials [10, 23, 24].

Ultrasonic waves, unlike light or electromagnetic waves, require an elastic medium like liquid or a solid to propagate. For this reason, the governing principles of acoustic waves are associated to material properties such as density and modulus of elasticity. The ultrasonic wavelength varies when the wave travels from one medium to another because of the elastic properties, which induces vibrations of the particles in the medium. Further, ultrasonic waves can be reflected off from very small surfaces owing to their much shorter wavelength. There are two types of ultrasonic waves: bulk waves and guided waves, which are found in a variety of applications [25, 26]. Bulk waves propagate wholly inside a material, independent of its boundary and shape, while guided waves propagate near the surface or along the interface of a material. According to the principles of the linear elasticity, ultrasonic waves are launched into the solid medium by different propagation modes out of which only two modes of interest are considered here for ultrasonic characterization: longitudinal waves (or compressional) and shear waves (or transversal). Propagation of ultrasonic wave can be described in terms of the direction of particles' motion in relation to the direction in which the wave propagates. Longitudinal waves are categorized based on their amplitude displacements which are parallel to the direction of travel. Shear waves are distinguished based on an amplitude displacement which is perpendicular to the direction in which the waves are traveling [25–29]. Therefore, understanding of the acoustic physics and analyzing the ultrasonic wave propagating into metals or alloys provide valuable information related to the microstructural features, mechanical properties, geometry, and thermomechanical history of the material [24, 27, 29–33]. Further, modern technologies which are capable of controlling all aspects of an ultrasonic wave afford greater possibility of measuring material properties and acoustic responses within different materials. These are the features which make ultrasound as the preferable technique over others for the nondestructive characterization of materials.

Ultrasonic parameters

During the propagation of ultrasonic wave in polycrystalline materials, waves interact with macroscopic, microscopic, and submicroscopic microstructural features of the material. Any derived information about the interaction between ultrasonic waves and microstructural features can be analyzed by ultrasonic parameters either alone or with a combination of ultrasonic parameters. These parameters are the propagating speed variations (or velocity), loss of amplitude (or attenuation), backscattered amplitude

[34–36], spectral analysis [37–39], and critical angles [8, 40]. Fundamental parameters of velocity and attenuation have been increasingly employed in the field of nondestructive characterization of material. Measurements of ultrasonic velocity and attenuation can explore the information about microstructural features since they are significantly affected by any changes in the microstructural features of the material.

Ultrasonic velocity

Velocity or speed of ultrasonic waves of any frequency and wavelength is associated to the characteristics of the material to be tested. The velocity of the wave varies with the physical properties of the medium when it passes through a medium. Therefore, the material properties can be calculated by measuring the velocity of an ultrasonic waves traveling through a material [27, 29, 33]. For velocity measurements, short ultrasonic pulses are introduced into the material at regular time intervals. By monitoring the reflected pulse, ultrasonic velocity can be determined by measuring the time of travel (Time of Flight [10]) between the two consecutive back-wall echoes, and dividing it by the distance traveled by ultrasonic wave. Different techniques have been used for velocity measurement such as pulse-echo overlap, pulse superposition, signals around techniques. Pulse–echo technique is the most popular for ultrasonic measurements wherein velocity can be accurately measured by considering the time required for a short ultrasonic pulse generated by a transducer to propagate through the thickness of the material [29, 41–44]. For example, in pulse–echo technique, velocity can be calculated by the well-known equation:

$$\text{Velocity (m/s)} = \frac{2 \times \text{thickness (m)}}{\text{time (s)}} \quad (1)$$

Regarding in situ applications, in order to avoid the error occurring during the thickness measurement, the ratio of longitudinal-to-shear velocity as parameter is used, instead; however, it reduces the sensitivity of measurements [37].

Ultrasonic attenuation

Ultrasonic attenuation refers to the loss of acoustic energy of ultrasonic waves as they penetrate through the material. Attenuation of ultrasonic waves is attributed to the different mechanisms such as reflection [45], diffraction [45], absorption [46], and scattering [47–52]. Absorption is the conversion of energy contained in the ordered particle's motion of the wave into disordered heat energy. Absorption is caused by microstructural defects such as dislocations and point defects, and by taking only small part of the measured attenuation in metallic materials and usually assumed to be negligible [45–47]. Scattering is described by the reflection of the sound waves in directions other than its original propagating direction. According to the theoretical model of attenuation, ultrasonic waves in a polycrystalline material are mainly attenuated by scattering at structural boundaries (grains, grain boundaries, inclusions, and pores) [47, 48]. The early work by Mason and McSkimin [49, 50] has introduced the grain-scattering model wherein the number of scattering is inversely proportional to the average grain volume. However, attenuation is a function of both grain size and frequency of ultrasonic wave. Stanke and Kino [51] and Weaver [52] have developed scattering-induced attenuation with equiaxial grains. The attenuation of ultrasonic waves in the material has been explained by the attenuation coefficient (α). The attenuation coefficient is the sum of the individual coefficients for scattering and absorption over all frequencies. Attenuation of ultrasonic wave can be measured as logarithmic decrement between the two consecutive back-wall echoes. Attenuation coefficient in pulse–echo technique can be calculated from the formula:

$$\text{Attenuation coefficient(dB/mm)} = \frac{20\log(S_1/S_2)}{2d} \quad (2)$$

where S_1 and S_2 are the amplitudes of two consecutive back-wall echoes, and d is the thickness of the specimen in (mm). In more advanced techniques, the attenuation coefficient at different frequencies can be obtained from the frequency spectrum (frequency vs. amplitude plot) of two successive back surface signals.

According to the above formulas, velocity and attenuation measurements depend on the accuracy of thickness measurement. There are also many factors affecting the accuracy of ultrasonic measurements such as calibration of equipment, coupling medium, and surface conditions of the test piece including roughness, curvature, and taper or eccentricity of the test piece [42]. The accuracy of any ultrasonic velocity and attenuation measurement is highly associated to the roughness and parallelism of test piece particularly in contact ultrasonic techniques. Surface roughness contributes to the inaccuracy in thickness measurements as well as in signal acquisition as highlighted by Fowler et al. [42]. However, Cong and Gang [38] introduced ultrasonic resonance technique based on spectral analysis for thickness measurement of nonparallel curves, with a good extent of accuracy (even in thickness less than 1 mm).

Application of ultrasonic evaluation techniques

As ultrasonic waves can be propagated into material and received by ultrasonic equipment, physical properties associated with elasticity of material can be measured.

Based on the pioneering works by Herzfeld and Litovitz [46], Mason [53], Truell et al. [54] and the subsequent works by Papadakis [47, 55–60], many ultrasonic measurement techniques and devices have been developed to evaluate the microstructural features and mechanical properties of materials in practical situations. It is worthy to note that most of researchers have dealt with ultrasonic velocity and attenuation measurements. Practically, ultrasonic techniques have been extensively deployed to accomplish a number of tasks:

(1) Determining the metallurgical properties like elastic constants such as Shear modulus (G), Bulk modulus (B), and Young's modulus (E) [27, 61–63].
(2) Characterizing the microstructural properties like measurement of grain size [41, 64–66].
(3) Determining the mechanical properties of materials like hardness [67, 68], yield strength [69, 70], ductile-to-brittle transition temperature [8, 71], and fracture toughness [72].
(4) Qualifying the processing treatments like measurement of recrystallization degree [73, 74] and measurement of case depth [75, 76].
(5) Evaluating the in-service degradations of material, like fatigue [77–80], creep [81], corrosion, and hydrogen damages [82, 83]; and measurement of residual stress [84–86].

Due to the well-established theoretical background, the specific focus of this review is specialized to studies which have been carried out by those who have implemented ultrasonic testing and evaluation methodologies for the characterization of microstructural variations during different thermal-treatment procedures. The different ultrasonic parameters have successfully been correlated with the microstructural variations induced by the heat treatments, such as phase transformation, phase precipitation, and aging–hardening reactions in a wide variety of materials like steels, stainless steel, super alloys, and aluminum alloys. Some of these studies are as follows.

Monitoring the phase transformation in carbon steels

Austenite decomposition is one of the most important metallurgical phenomena in carbon steels which determines microstructural and mechanical properties of the final product to a considerable extent. During cooling of carbon steels, *FCC* iron (or austenite) decomposes into more stable iron–carbon compounds like ferrite, pearlite, and bainite [87–89]. Many attempts have been made to observe the phase transformations during the austenite decomposition of carbon steels with different carbon contents at low or high temperatures through ultrasonic measurements [89–97]. Totally, it is found that ultrasonic wave parameters, particularly velocity and attenuation, vary considerably during austenite decomposition and are able to provide real-time information on the kinetics of phase transformation.

The ultrasonic velocity behavior of each steel phase is found to be a linear function of the temperature [89, 90]. Figure 1 illustrates a general form of the velocity–temperature curves for austenite (γ) and ferrite (α) phases in 1008 steel [89]. It can be seen that the velocity-temperature variation in the austenite range (γ-region) is mostly linear. During the austenite decomposition (850–750 °C), the velocity dependence on temperature is almost linear but with a different slope than that of γ range. The slope of the velocity variation in the γ phase is reported to be not mainly dependent on the carbon content [89, 90]. One important feature of linear behavior in velocity–temperature curve is the Curie temperature of ferrite ($\approx$770 °C) where velocity is no longer linear in the temperature below 770 °C (Fig. 2). The Curie temperature of ferrite is the temperature where the magnetic properties shift from paramagnetic (austenite) to ferromagnetic (ferrite). This ferromagnetic–paramagnetic transition of iron clearly affected ultrasonic velocity, and the precise velocity measurements can be done only at temperatures less than the Curie temperature where the velocity difference between phases is larger [89, 90].

Dubois et al. [90] have reported a hysteresis in the velocity–temperature curve in hot-rolled carbon steels associated with the austenite–ferrite/pearlite phase transformations (Fig. 3). For instance, two temperature features can be observed in velocity–temperature curves of 1035 steels at 690 and 650 °C which are associated to the austenite-to-ferrite and austenite-to-pearlite transformations, respectively. During heating, these phase transformation temperatures are higher than the equilibrium

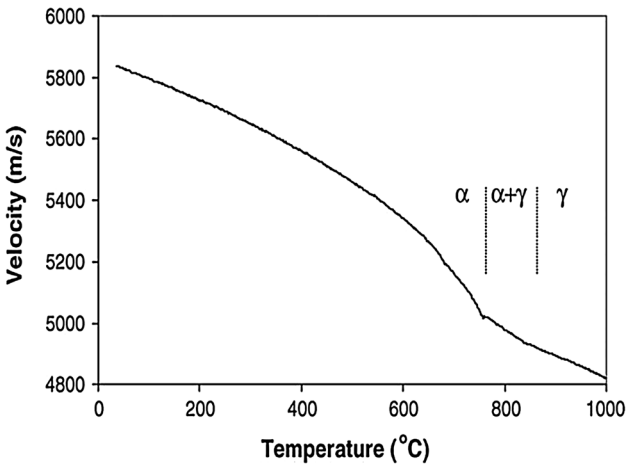

Fig. 1 Velocity dependence on temperature for various phases in 1008 steel [89]

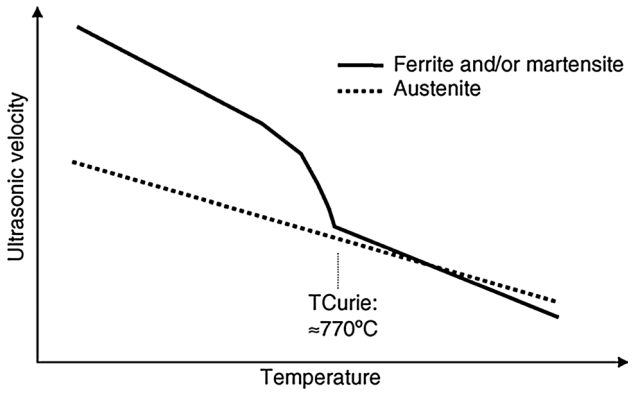

Fig. 2 Longitudinal wave velocity as a function of temperature in 1008 steel [89]

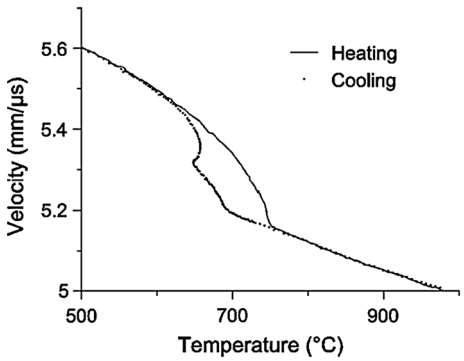

Fig. 3 Ultrasonic velocity curve in a 1035 steel sample during heating and cooling [90]

transformation temperatures, while being lower during cooling. However, it must be noted that the occurrence of these phase transformations is related to the steel grades. They found local minima in ultrasonic velocity and attenuation corresponding to the phase transitions. Therefore, the velocity behavior identifies the start and end of phase transformations, even allowing for discrimination between ferrite and pearlite nucleations.

It is also known that the ultrasonic measurements are dependent on the microstructural variations induced by heat treatment in steels with different carbon contents where the constituent phases significantly affect the ultrasonic parameters: velocity and attenuation. In fact, variations of both velocity and attenuation of ultrasonic waves reflect changes in microstructure during the austenite decomposition [7, 98, 99]. According to Freitas et al. [7], Fig. 4, various microstructures have different ultrasonic velocity values where the martensite possesses the lowest ultrasonic velocity and ferrite the highest. These results were also confirmed by Gür and Tuncer [98], Gür and Cam [99], Papadakis [59, 60], and Grayali and Shyne [100]. Due to the compact and fine granulation of martensite microstructure, it offers more resistance to the propagated ultrasonic wave compared with the pearlite and ferrite microstructures [61]. Ferrite presents the least resistance to ultrasonic waves because of equiaxial and large grain size, which facilitates facile propagation of ultrasonic wave [98]. It has been found by Albuquerque et al. [101] that the finer the grain sizes, the lower the ultrasonic velocity, while the opposite behavior is found by Palanichamy et al. [41]. Also it is known that coarse pearlite is less resistant to propagated ultrasonic waves in relation to fine pearlite because of its large lamellar spacing [7]. A few studies have investigated the effect of austenitic grain size on ultrasonic parameters of various steels [41, 60, 102]. They have reported that finer prior austenitic grain size reduces the ultrasonic velocity. An increase in grain boundary areas causes ultrasonic waves to take a longer path to cover the material thickness and further scatters the ultrasonic waves [41]. Furthermore, ultrasonic velocity measurements are found to be sensitive to the carbon content of the material, where the higher carbon content decreases the ultrasonic velocity [7, 61]. However, there is no information so far about the correlation between ultrasonic attenuation and carbon content as reported by Bouda et al. [31, 66]. Besides the grain size effect, ultrasonic velocity is also dependent on the frequency of ultrasonic wave as reported by Hirsekorn [103, 104].

Gür and Tuncer [98] and Gür and Çam [99] tried to eliminate the effect of grain size and nonuniformity of the microstructure in order to understand only the relationship between phase transformation and velocity in steels. They applied a precise heat-treatment procedure to obtain the specimens with an identical average grain size and a microstructure with no texture. Similarly, velocity of longitudinal and shear waves were found to be lowest in martensite as a hardest phase, intermediate in the bainite, and highest in coarse pearlite–ferrite as a softest phase [98, 99]. The lowest velocity values of martensite have been interpreted by the high amount of internal tension caused by distortion of crystal lattice due to the transition from austenite phase (FCC) into the martensite (BCT). The transformation of austenite into martensite occurs by diffusionless lattice shear where austenite suddenly changes to long and thin laths of martensite. This transformation increases the quantity of lattice distortion and elastic anisotropy in the prior austenite grains [7, 98, 99, 105]. The higher velocity of other phases is due to the lower lattice distortion and misorientation in the prior austenite grains than those of martensite [100]. The velocity of pearlite–ferrite microstructure is influenced not only by lamellar spacing but also by the size and the content of ferrite. Larger spacing of the cementite lamellae–ferrite and higher quantity of ferrite provide higher velocity values. Moreover, the lower velocities of fine pearlite–ferrite compared

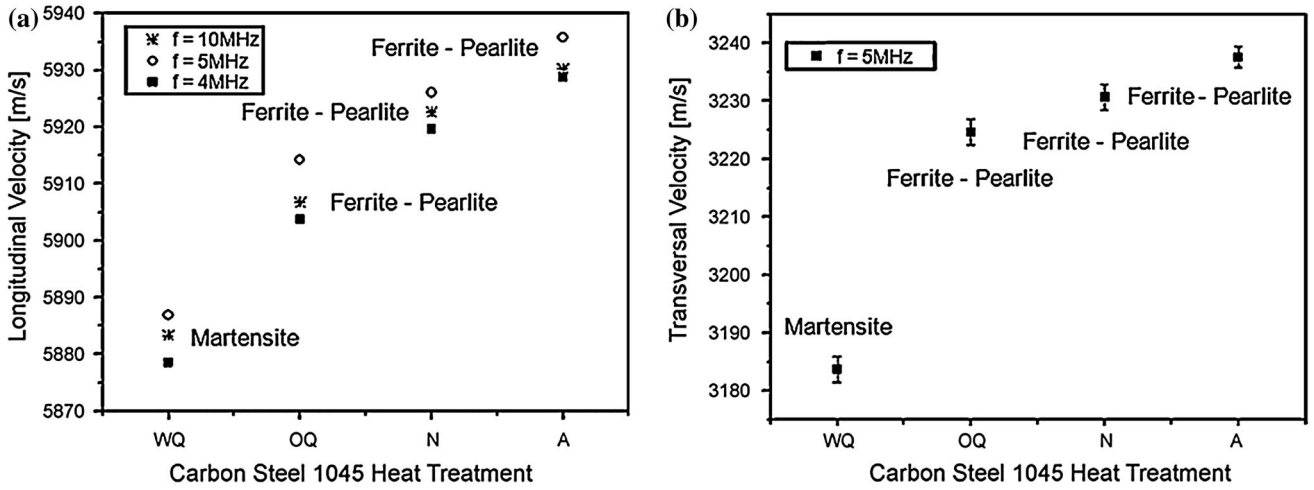

Fig. 4 Longitudinal (**a**) and transverse (**b**) ultrasonic velocity measurements for AISI 1045 [7]

with the coarse pearlite–ferrite has been attributed to the lower size and quantity of ferrite and shorter lamellar spacing as can be seen in Fig. 5.

Besides the homogeneous elastic lattice deformation, austenite transformation is accompanied by a significant increase in dislocation density. A few studies have shown the effect of plastic deformation level and subsequent heat treatments on the ultrasonic properties [95, 105]. It has been reported that the increase in the degree of deformation results in the increase in dislocation density and thereby decreases the ultrasonic velocity. Hardened material by deformation presents lower ultrasonic velocity than the annealed and normalized materials (maximum velocity) [96, 105]. The lower velocity is attributed to the lattice distortion as a result of higher dislocation density. Annealing heat treatment even at modest temperatures increases ultrasonic velocity as a result of the lower dislocation density and lattice distortion under the annealed condition as reported by Prasad and Kumar [106].

The velocity of the ultrasonic waves in the polycrystalline or bulk materials is primarily controlled by the elastic modulus and the density which in turn are related to the microstructure through variations in the elastic modulus of the individual grains, the orientation of the grains, and relative amounts the phases present [60, 98, 99, 106]. According to Gür and Tuncer [99], ultrasonic wave is mainly associated to the elastic modulus rather than density since they found an inverse relation between velocity and

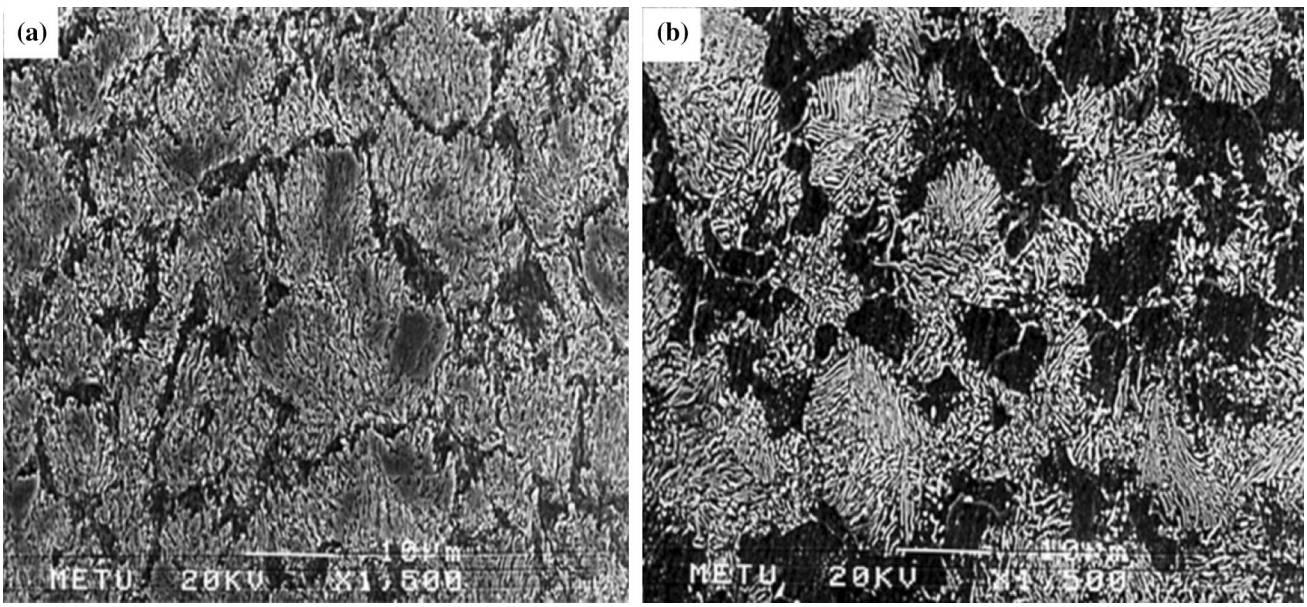

Fig. 5 SEM micrographs of heat-treated AISI 4140: **a** fine pearlite–ferrite, **b** coarse pearlite–ferrite [98]

density. In general, a substructure which strains the lattice or interrupts the matrix continuity reduces the elastic modulus and velocity of ultrasonic waves [59, 98]. Kumar et al. [107–109] have attributed variations in ultrasonic velocity to the precipitation behavior of the 9 % chromium ferritic steel subjected to aging. As can be seen in Fig. 6, corresponding to the intercritical region (between Ac_1 and Ac_3 temperatures), ultrasonic velocity decreases sharply as a result of increased volume fraction of martensite in the structure caused by increasing the soaking temperature. The lower velocity of martensite phase has been related to the lower elastic modulus compared to that of ferritic structure. This increased volume fraction of martensite is also reflected in the variation in the hardness. A direct correlation between velocity and hardness has been previously reported by Badidi et al. [66]. Therefore, ultrasonic velocities have been found to be able to identify the critical Ac_1 and Ac_3 temperatures as well as to determine of hardness variation in intercritical region. Above the Ac_3, the velocity remains almost constant which is due to the similar microstructure existing in this region. As soaking temperature increases, the velocity decreases as a result of the finer grain size of microstructure as explained earlier.

Since the ultrasonic velocity variation arises from the variation in the elastic modulus of material, different elastic constants of the material can be calculated from the relation between longitudinal velocity (V_L), shear velocity (V_S), and the density of the material (ρ) according to the following empirical formulas [110]:

$$\text{Longitudinal modulus}(L) = \rho V_L^2 \tag{3}$$

$$\text{Shear modulus}(G) = \rho V_S^2 \tag{4}$$

$$\text{Bulk modulus}(B) = \rho\left(V_L^2 - \frac{4}{3}V_S^2\right) \tag{5}$$

$$\text{Young's modulus}(E) = \frac{\rho V_T^2\left(3V_L^2 - 4V_S^2\right)}{V_L^2 - V_S^2} \tag{6}$$

$$\text{Poison's ratio}(v) = \frac{V_L^2 - 2V_S^2}{2\left(V_L^2 - V_S^2\right)} \tag{7}$$

Ultrasonic attenuation behavior has been also found to reflect the microstructural variations during austenite decomposition transformation. Average prior austenite grain size and various phases existed in the microstructure: their morphology and distribution influence the attenuation behavior [96, 101, 102, 107, 111]. The attenuation variation is primarily due to the wave scattering through the material grains [101]. It has been stated that scattering is the predominant mechanism compared with true absorption in the attenuation of propagated ultrasonic waves in polycrystalline materials such as austenitic stainless steel [41]. However, it must be noted that attenuation is also affected by various microstructural parameters such as phase transformations [96, 102, 107, 111].

Dubois et al. [91] have observed fluctuation in variations in the ultrasonic attenuation during heating and cooling of the A36 and in IF steels (Fig. 7). They claimed that attenuation variations during phase transformations arise primarily from changes in the grain size [60, 91]. They witnessed the drop in attenuation values in the phase-transformation temperature range or intercritical region (between Ac_1 to Ac_3) dominated by finer microstructure than the prior ferritic structure. In contrast, heating above the 1050 °C causes a remarkable increase of attenuation as the austenite grains grow. In fact, the larger austenite grains increases the ultrasonic attenuation. It is known that scattering is proportional to the prior-austenite grain volume, particularly in the Rayleigh scattering region [112]. According to the scattering theory, the relation between attenuation and grain size relies on the ratio of the acoustic wavelength, λ, to the average grain size, D [91].

As mentioned earlier, the attenuation is affected by various microstructural constituents during phase transformations. By considering the same prior austenite grain size, martensite has been found to be the most attenuating

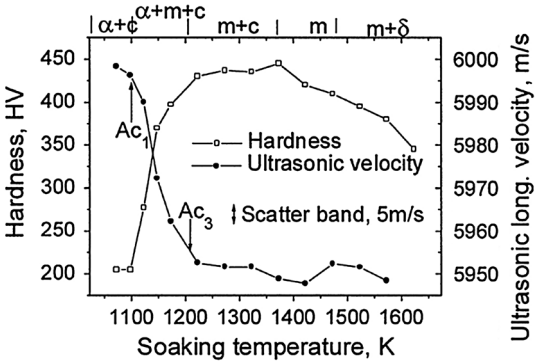

Fig. 6 Effect of microstructural variation on ultrasonic longitudinal wave velocity and hardness [107]

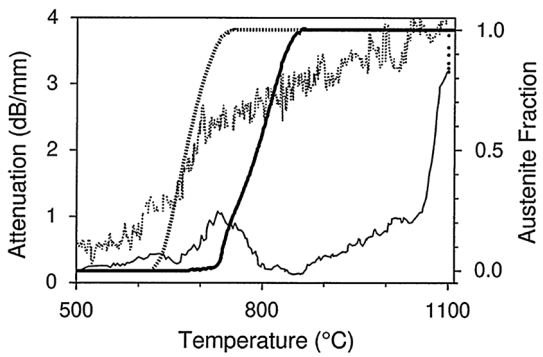

Fig. 7 Ultrasonic attenuation as a function of temperature in an A36 steel [91]

microstructural phase, and thick ferrite–pearlite to be the least attenuating [7]. The similar trend of velocity for phase transformation has been found in the attenuation measurement where attenuation coefficient increases in the order of martensite, bainite, pearlite and its associated phases; ferrite and cementite [7, 108–110].

Based on Kumar et al. [109] showed that breaking down of martensitic laths present in the microstructure of 9Cr-1Mo ferritic steel into a finer structure decreases the acoustic impedance difference between two adjacent grains, thereby making the structure more anisotropic, and reducing the scattering. Obviously, the overall attenuation is mainly influenced by scattering and not by dislocation damping as reported by Kumar et al. [109]. It has been observed that the ultrasonic attenuation varies in the same manner as grain size varies with soaking temperature (the lower the grain size, the lesser the attenuation) [108, 109]. Further, Kumar et al. [108, 109] have correlated the attenuation behavior with the precipitation behavior of the 9 % Cr ferritic steels. By the dissolution of precipitates (V_4C_3 and NbC carbides), the attenuation increases, whereas as a consequence of α-ferrite formation, the growth of grains decreases and, thus, the attenuation decreases.

Besides the velocity and attenuation measurements, other ultrasonic parameters such as ultrasound absorption [93, 94], spectral analysis [108–110], and ultrasonic backscattering [36, 40] have been employed by researchers to study the phase transformation of steels. Lamouche et al. [93] and Kruger et al. [94] conducted experiments based on ultrasound absorption measurement to monitor microstructural evolution during heat treatment of medium-carbon steels. Both references cited represented high reliability of ultrasonic absorption measurements to monitor the microstructural evolution of steel in various temperature ranges. Lamouche et al. [93] have proposed a combination of laser ultrasonic with the reverberation technique. However, their combined technique is restricted to finite-sized samples, and consequently, it is not practical in an industrial environment, except for very special cases. The interactions of ultrasonic waves with the microstructural features and inhomogeneities yield variation in frequency distribution of wave (spectral analysis) or creating backscattered signals (backscatter spectral analysis). Such inhomogeneities are grain boundaries, porosity, precipitates, inclusions, and other microstructural components with acoustic impedances different from that of the matrix, which behave as scattering points [35, 36, 113]. Spectral analysis has been successfully used for the assessment of the grain size, in order to identify different metallurgical features in steels through the evaluations of frequencies and amplitudes of ultrasonic wave signals [114]. Kumar et al. [109, 110] have found that the spectral peak ratio (SPR) increases with the increasing grain size, which follows the same trend as that of the attenuation. In fact, spectral analysis is used for the evaluation of the waveform of ultrasonic wave which has been sent through a material. This is because, as ultrasonic wave is further propagated into the material, the ultrasonic wave is attenuated, and consequently the oscillatory amplitude decays exponentially [108, 109]. Leviston and Bridge [40] have shown that the backscatter technique?? based on the Rayleigh angle can distinguish different microstructural features induced by heat treatment in steels. Backscattered signals carry useful information about the microstructure and its spatial distribution; however, it needs nonconventional statistical methods [36, 115]. The main advantage of the backscattering technique over attenuation and velocity techniques is that no acquired back-wall echo is needed. Therefore, characterization of rough, nonparallel, and unknown thickness could be easily realized [35–37, 113].

Finally, it has been concluded that ultrasonic measurements have great potential for real-time characterization of the phase transformations taking place in different steels. Both velocity and attenuation are significantly affected by the temperature and constituent phases of the steel microstructure. Ultrasonic velocity is mainly decided by the variations in the elastic modulus which is associated to the degree of lattice distortion and misorientation in the prior austenite grains, while ultrasonic attenuation is associated to grain size and various phases in steels. Further, ultrasonic velocity measurements seem to be much easier than attenuation measurement because the causes of velocity variations in steels are simple to understand. In addition, using higher-frequency transducers offer better correlations of both ultrasonic attenuation and velocity with microstructural variation due to the relatively shorter wavelengths of high-frequency ultrasonic waves; therefore, greater sensitivity to microstructural objects like grains is expected [63].

Phase variation during solutionizing of stainless steel grades

Cast austenitic stainless steel (CASS) as a polycrystalline coarse-grain material is routinely used in the nuclear power industry. Ramuhalli et al. [116] and Anderson et al. [117] have effectively used the ultrasonic measurements for the characterization of CASS. Ramuhalli et al. [116] have proposed that the velocity and diffused ultrasound measurements can potentially be used to identify the material type and the microstructural class of CASS. Ultrasonic measurements have been found to be useful in the classification of grain structure in a microstructure consisting of equiaxed and columnar grains. Hsu et al. [118] have reported that velocity is proportional to the modulus of

elasticity of martensitic stainless steel where the ultrasonic velocity increases by increasing the modulus of elasticity. It must be noted that both velocity and modulus of elasticity increase by tempering treatment. It is known that propagation of acoustic waves in equiaxed-grain materials depends on the texture and related degree of anisotropy [116, 117]. The cast stainless steels exhibit considerable attenuation compared with the tempered, heat-treated ones, which is attributed to the presence of carbide films at grain boundaries. These carbide films delayed the elastic deformation of the material and caused a scattering of the ultrasonic waves.

Vijayalakshmi et al. [119] and Jayachitra et al. [120] studied the effects of annealing temperature and induced microstructural features on ultrasonic parameters of a duplex stainless steel (DSS). When DSSs are subjected to the thermal cycle, they undergo complex microstructural transformations, affecting the ferrite–austenite ratio (α/γ), morphology, and grain size in the microstructure (Fig. 8) [119].

Both the references cited illustrate that velocity is affected by a combination of the ferrite content and grain size; while the attenuation is purely decided only by the grain size, wherein attenuation is directly proportional to grain size as reported by Kumar et al. [108]. The variations of both attenuation and grain size of 2205 DSS with solutionizing temperature are shown in Fig. 9. By increasing the temperature, the attenuation remains unchanged within the two-phase region ($\alpha + \gamma$), but with the increasing temperature in the single-phase region (α, above the solvus line), the attenuation rapidly increases even with small increase in the temperature. The more or less constant

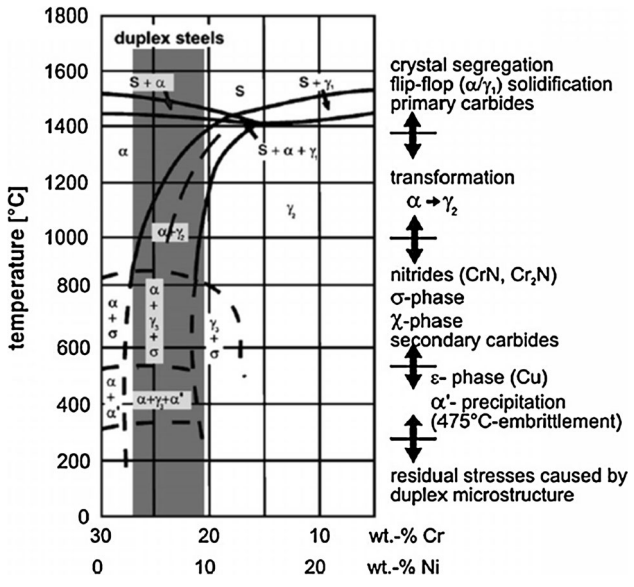

Fig. 8 Pseudo-binary Fe–Cr–Ni phase diagram for 70 % Fe [119]

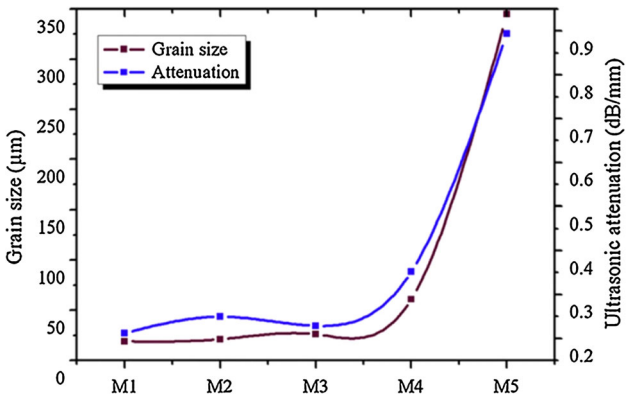

Fig. 9 Variations of attenuation and grain size with solution-treated temperature [119] (Note that M4 ≅1300 °C)

values of attenuation within the two-phase region are attributed to the stronger effect of microstructural morphology than grain size. The microstructures in the two-phase region consist of fine and uniform distribution of ferrite (α) and austenite (γ), which leads to relatively constant grain size. Above the solvus line (M4 point), the material experiences grain coarsening as a consequence of formation of 100 % ferritic microstructure during solutionizing at higher temperature, wherein the attenuation increases with the temperature [119]. Jayachitra et al. [120] by increasing the holding time at 1300 °C have confirmed that attenuation is independent of relative amount of phases and their morphology.

Different behaviors of longitudinal velocity and shear velocity have been observed in the two-phase region by Vijayalakshmi et al. [119]—where longitudinal velocity decreases, while shear velocity remains almost constant. As the solution temperature increases, the volume fraction of ferrite increases which has been found to contribute to the increase in the longitudinal velocity after initial decrease. Above the solvus line, increases in ferrite content and grain coarsening are expected; therefore, both longitudinal and shear velocities decrease with grain coarsening [120]. It is clear that velocity behavior is dependent on both ferrite–austenite ratio and the grain size where both parameters show opposite effects on velocity behavior. The increase in the amount of ferrite through the dissolution of austenite dominates the influence of grain coarsening behavior in the both velocities [120]. Further, Jayachitra et al. [120] has pointed out that both longitudinal and shear velocities are directly proportional to E or G, while K and ν values are inversely proportional to the ultrasonic velocities. It is noted that velocity increases with the increasing E or G values. However, for isotropic solid materials, shear velocity has depicted a better correlation with elastic properties than longitudinal velocity, which is also reported by Kumar et al. [121].

Finally, it is evident that both attenuation and velocity in solution-treated DSS are decided by the solution treatment temperature. Velocity is affected by the combined effect of the ferrite content and grain size; however, ferrite content has stronger effect on longitudinal velocity compared with the grain size. Attenuation is purely correlated only with grain size and is directly proportional to grain size.

Characterizing of age or precipitation-hardened alloys

The mechanical properties of precipitation-hardened alloys, such as aluminum-, iron (ferritic and maraging steels)-, and nickel-based superalloys are determined through age-hardening phenomenon or more often called the precipitation hardening. Precipitation hardening is the predominant mechanism of strengthening in such alloys through the controlled formation of an ordered precipitate structure [63, 122–124]. Characterization of precipitation-hardening alloys has been carried out by using the ultrasonic parameters as discussed below.

Precipitation hardening in aluminum alloys

Several studies exclusively have characterized the age hardening of wrought aluminum alloys [125–131]. In general, variations of ultrasonic properties as a function of aging time and temperatures are found to be associated to the hardening of the aluminum structure [132]. Tariq et al. [126] have demonstrated that longitudinal velocity increases as aging time increases and nonmonotonically follows the similar trend as that of hardness in the response to aging. The same trend in the variation of velocity with aging treatment has also been quoted earlier by other researchers [129–133]. For instance, the prominent features of the variation in velocity as a function of aging are depicted in Fig. 10 [126]. Both longitudinal velocity and hardness increase to a certain peak value and then decrease under over-aging condition. The variations in velocity values with the extent of aging are attributed to the precipitation of various metastable phases during aging, irrespective of the type of the precipitate [62, 126–131]. Extensive precipitations of different types of strengthening phases cause hardening of the matrix and contribute to the increase in ultrasonic velocity during aging. In fact, the variations in velocity during precipitations of different intermetallic phases are associated with variations in the elastic modulus of the alloy matrix which in turn change with age hardening due to the compositional variations [126, 128, 133]. Rosen et al. [133] have indicated that the elastic modulus increases with the increasing aging temperature. Initially, both hardness and ultrasonic velocity increase as a result of the breakdown of supersaturated solid solution (SSSS), formation of co-clusters, and other

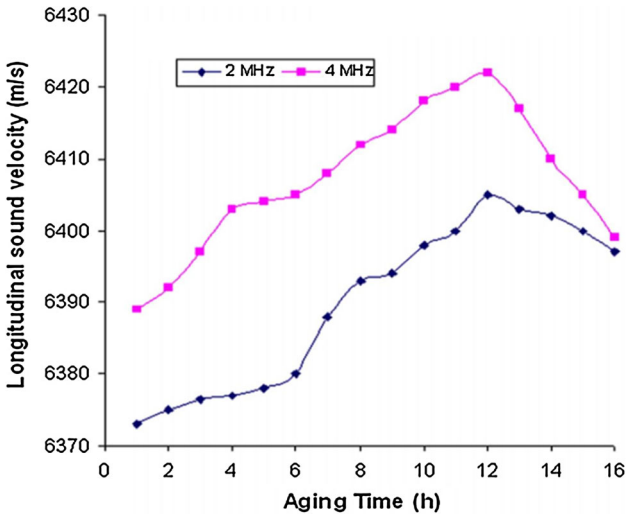

Fig. 10 The variation in longitudinal velocity with aging time for AA 2014 [126]

intermediate phases. The depletion of the precipitate-forming elements from the matrix, formation and growth of co-clusters, and (GPB zone) increase the modulus of the matrix and in turn increase the ultrasonic velocity [128]. Murav'ev [134] has attributed the increase in the ultrasonic velocity to the reduction in the extent of distortions of the crystal lattice due to increased volume fraction of precipitates.

The substantial volume fractions of intermediate precipitates of intrinsically higher elastic modulus than the matrix result in a net increment of the elastic modulus of the aged specimen, thus contributing to the peak velocity condition [126, 128–136]. Longitudinal wave velocity values are found to be decreased with the onset of the over-aging condition wherein coherent precipitates are dissolved and the noncoherent precipitates are formed at the expense of the elastically rigid coherent phases which reduce the average modulus of elasticity, and in turn, the ultrasonic velocities [126, 128]. In fact, the variations in ultrasonic velocity with aging arise primarily from the differences in the elastic modulus of the precipitates and precipitate/matrix interface which in turn depends on precipitation process [131–133]. Furthermore, the occurrence of various peaks (dip) in the velocity with aging time (Fig. 10) is representative of sequential, although possibly independent, stages of precipitations as observed by others [126, 135, 136].

The behavior of attenuation can be explained by the precipitate sizes and the states of coherency between precipitates and matrix [115, 131–133, 136]. An example of attenuation's variation with aging treatment is shown in Fig. 11 [126]. The main contribution to the attenuation is believed to be from the scattering of the ultrasonic wave by

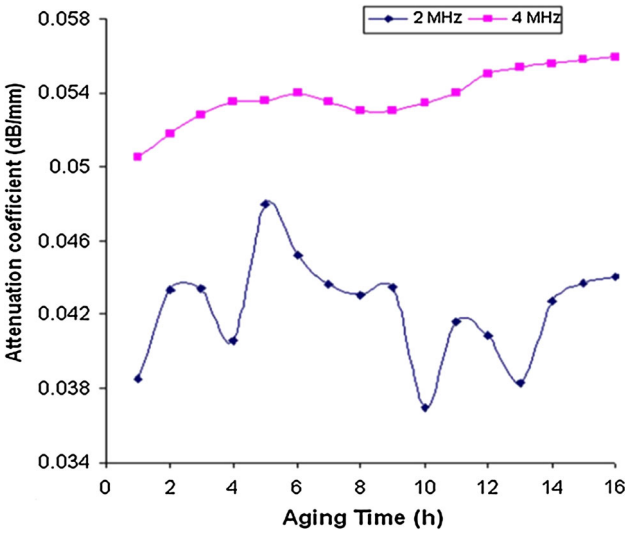

Fig. 11 The variation of attenuation coefficient with aging time for AA 2014 [126]

the newly formed precipitates which act as scattering points in the path of propagating wave, which increases the attenuation coefficient of waves during aging. As aging proceeds further, precipitates with different impedances than that of matrix are formed, which scatters the propagated ultrasonic waves and so increases the attenuation of ultrasonic waves [131–133]. The initial increase in ultrasonic attenuation is attributed to the purification of the matrix through the segregation of the solute atoms and formation of GP zones, and other metastable phases during aging as reported by Muthu Kumaran [128] and Rosen et al. [131, 133],. Further increase in the scattering of waves and so the attenuation by coarsening of precipitates in the over-aging condition is expected. The dependence of ultrasonic attenuation on precipitations of various intermetallic phases during aging and coarsening processes of precipitates in over-aging is reported in Gefen et al. [125, 127], Gür and Yildiz [137], and Stanke and Kino [49].

In conclusion, the behavior of ultrasonic parameters can be interpreted by the microstructure, size, distribution, and volume fraction of precipitates; however, the degree of structural and crystallographic coherency with the matrix does not influence ultrasonic measurement in aluminum alloys. Ultrasonic measurements are found to be effective in the determination of the different aging conditions and their microstructural states. Velocity measurements have shown better correlation with microstructural states where different stages of precipitation can be predicted with a good extent of accuracy.

Formation of precipitates in superalloys

A few studies have already been done regarding characterizations of the microstructural variation and the formation of the secondary phases due to thermal aging in the nickel-based superalloys particularly Inconel 625 through ultrasonic measurements [63, 138–143]. By the correlation analysis of microstructural variation and ultrasonic velocity, it has been found that ultrasonic velocity increases with the formation of precipitates, whereas dissolution or coarsening of precipitates decreases the velocity as the aging proceeds [63, 138, 140–142].

Figure 12 shows the variation of longitudinal velocity with annealing temperature of nickel-based and zirconium-based superalloys. As can be seen in Fig. 12a, velocity increases with the increasing aging temperature, reaching to a peak at around 700 °C and decreases with further increase in aging temperature [140]. Upon subjecting the

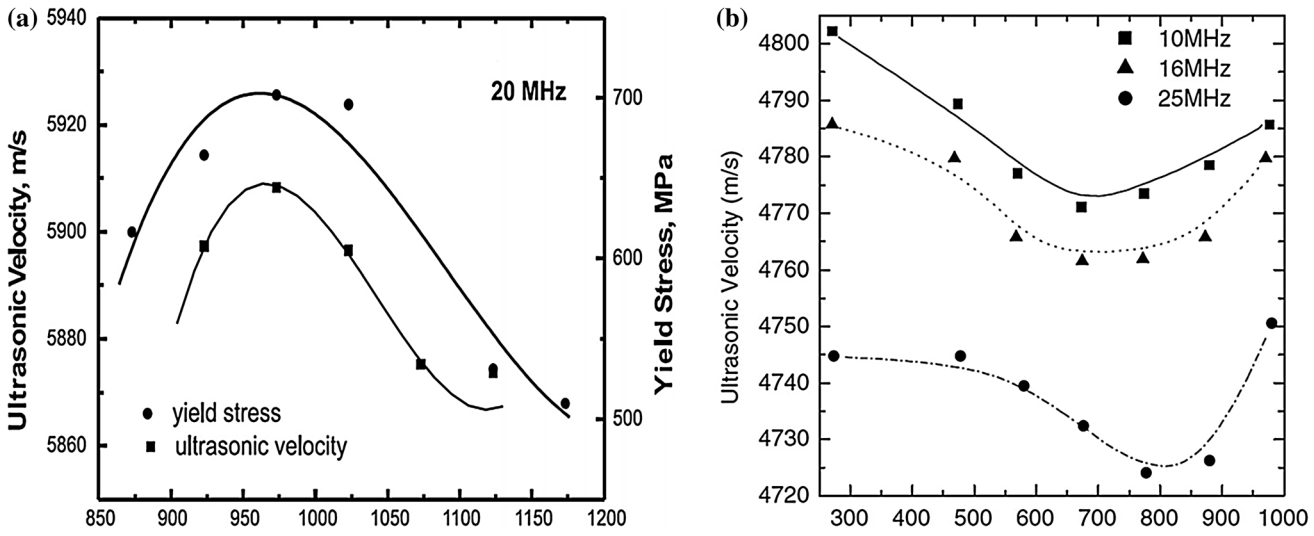

Fig. 12 The variations of longitudinal velocity with annealing temperature of **a** Inconel 625 [140] and **b** Zircaloy-2 [145]

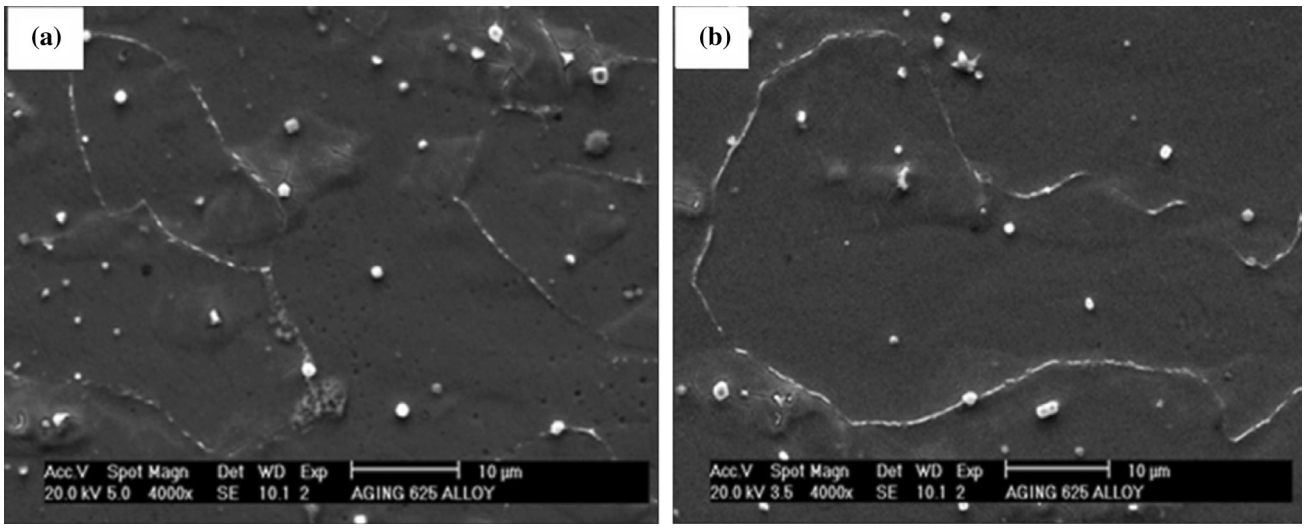

Fig. 13 SEM micrographs of aged Inconel 625 specimens showing the precipitation of second phases in the matrix (**a**) and grain boundaries (**b**) [139]

annealed Inconel 625 to the aging or elevated temperature, it experiences the precipitations of γ'' (Ni_3 (Nb, Al, Ti)), Ni_2 (Cr, Mo) and intermetallic δ-phases [Ni_3(Nb,Mo)], as well as the formation of networks of carbides on grain boundaries occurs (Fig. 13) [138, 147]. The increase of velocity linearly with the volume fraction of γ' precipitates has also been reported in Nimonic alloy [148–151]. The similar response of ultrasonic velocity to precipitation has been found in aluminum alloys as mentioned earlier. The decrease in the ultrasonic velocity as a result of the precipitation of intermetallic phases has been reported in zirconium-based superalloys, Fig. 12b [144–146].

The compositional changes due to the formation and the dissolution of intermetallic precipitates have been found to contribute to the increase in the elastic modulus alloy and thereby the ultrasonic velocity [63, 140, 148–150]. In this case, the similar behaviors in the variation of both Young's modulus and ultrasonic velocity have been observed by Palanichamy et al. [142] and Jayakumar et al. [151]. In fact, the precipitation process of intermetallic phases upon aging can be divided into two stages: incubation period and precipitation. During the incubation period, the excess solute atoms migrate to certain crystallographic planes and form the clusters or embryos of the precipitate. Upon precipitations, clusters form an intermediate crystal structure or transitional lattice which maintains the coherency with lattice structure of the matrix. These precipitates or phases having lattice parameters different from those of the matrix result in a considerable distortion of the matrix. Murthy et al. [148–150] have demonstrated that the first stage of the precipitation—the depletion of the precipitate-forming elements from the matrix—increases the modulus of the matrix and in turn increases the ultrasonic velocity;

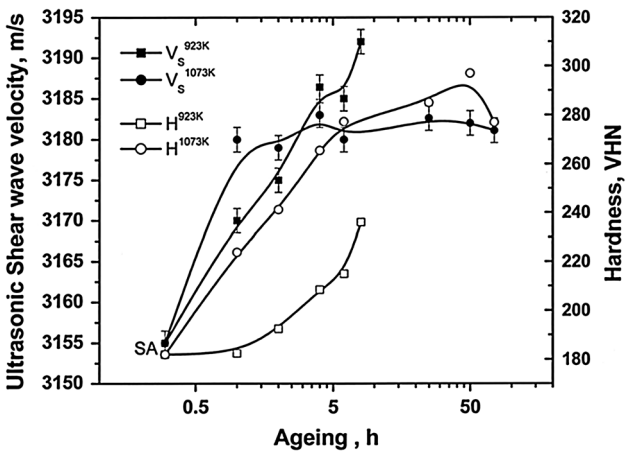

Fig. 14 Variations in longitudinal velocity and hardness with aging in Nimonic 263 [149]

however, it does not influence the hardness significantly (Fig. 14).

The precipitation of γ' phase in Nimonic alloy results in depletion of the precipitate-forming elements from the matrix, which contributes to significant increment of the elastic modulus upon aging, as explained earlier. However, it is found that the growth of γ' phase and its conversion to acicular η phase do not affect the ultrasonic behavior because it does change the matrix composition [148–150]. Further, Murthy et al. [149] has observed the higher value of velocity in specimen aged at 700 °C compared with the specimens aged at 800 °C, which is related to the higher solubility of precipitate-forming elements at higher temperature (Fig. 14). There is a point in velocity measurements showing that shear velocity has been found to be more sensitive to the precipitation of

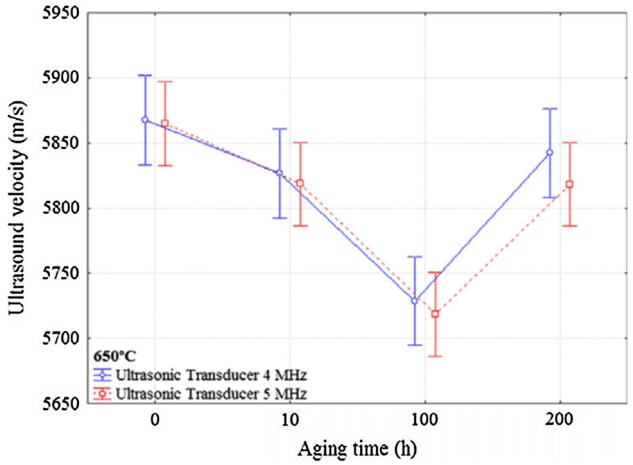

Fig. 15 Ultrasonic velocity variation with aging time at 650 °C in Inconel 625 alloy [139]

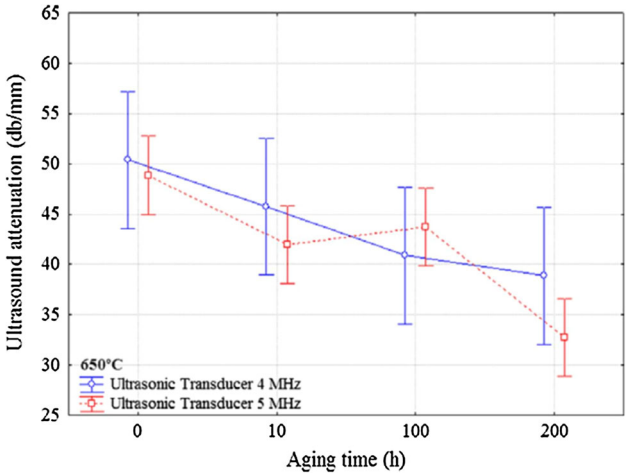

Fig. 16 Ultrasonic attenuations variation with aging time at 650 °C in Inconel 625 alloy [139]

intermetallic phases compared with longitudinal velocity [63, 138, 142, 151].

De Albuquerque et al. [139] have also observed the effects of different stages of colloidal precipitation on velocity, Fig. 15. They indicated the presence of two stages of precipitation: (1) dissolution of the Nb-rich Laves phases over shorter aging time and (2) formation of cuboidal precipitates rich in Ti and Nb over longer aging time. The initial decrease in velocity has been attributed to the dissolution of precipitates formed after welding, while the velocity starts to increase upon precipitation of new phases, or variation in the volume fraction of precipitates. Depending on the temperature ranges, different types of precipitates and even grain boundary carbides (Fig. 13) dissolve during the aging [147]. However, Kumar et al. [142] reported that the ultrasonic velocity is influenced only by the precipitation of intermetallic phases, and not by the grain-boundary carbides.

The opposite behavior of velocity has been found in the ultrasonic attenuation behavior wherein attenuation values continuously decrease as a result of the dissolution of the Laves phases and further by considerable precipitation of phases rich in Ti and Nb (Fig. 16). Various precipitates cause the scattering of sound wave which in turn leads to the variation of attenuation values [138, 139]. Shah et al. [141] have shown a higher attenuation in aged samples compared with virgin sample due to the presence of precipitates. Similarly, Kumar et al. [152] have reported the increase in the attenuation during the re-solution annealing (RSA), where the dissolution of the precipitates along with grain growth occurs during RSA.

In conclusion, the above-mentioned correlations demonstrate that the ultrasonic velocity and attenuation can follow the phase transformations during aging or elevated temperature exposure of superalloys because they are affected by the microstructural variations in terms of differences in the precipitations formed and their morphologies. Any other variations in the microstructure, such as grain coarsening, can be readily detected by the attenuation measurement.

Characterization of thermal-aging degradation

Long-time exposure at high temperature leads to degradation of microstructural and mechanical properties of in-service materials and components due to aging. Ultrasonic parameters are frequently being used to evaluate the performance of components during high-temperature service. The followings are some of these studies.

Characterization of the thermal embitterment of duplex stainless steels (DSSs)

Embrittlement is one of the common degradation mechanisms of DSSs as a result of phase transformation. When DSSs are subjected to temperature above 300 °C such as in welding, they are susceptible to precipitation of various phases such as alpha line (α') and sigma phase (σ) over the ferritic microstructure (matrix) depending on the temperature range [153–156]. Pohl et al. [157] have also reported the precipitation of σ along with χ (Mo-rich) and secondary austenite (γ_2) through a eutectoidal reaction $\delta \rightarrow \sigma + \gamma_2$ in the temperature range between 650 and 900 °C. At less than 550 °C, the α' phase accounts for the embrittlement, while embrittlement occurs due to precipitation of the σ phase at greater than 550 °C because the higher kinetics of embrittlement prevents the formation of the α' phase [152, 153]. Studied temperature range is characterized by the spinodal decomposition wherein α-initial phase transforms of into α-phase poor in chromium and α'-phase rich in

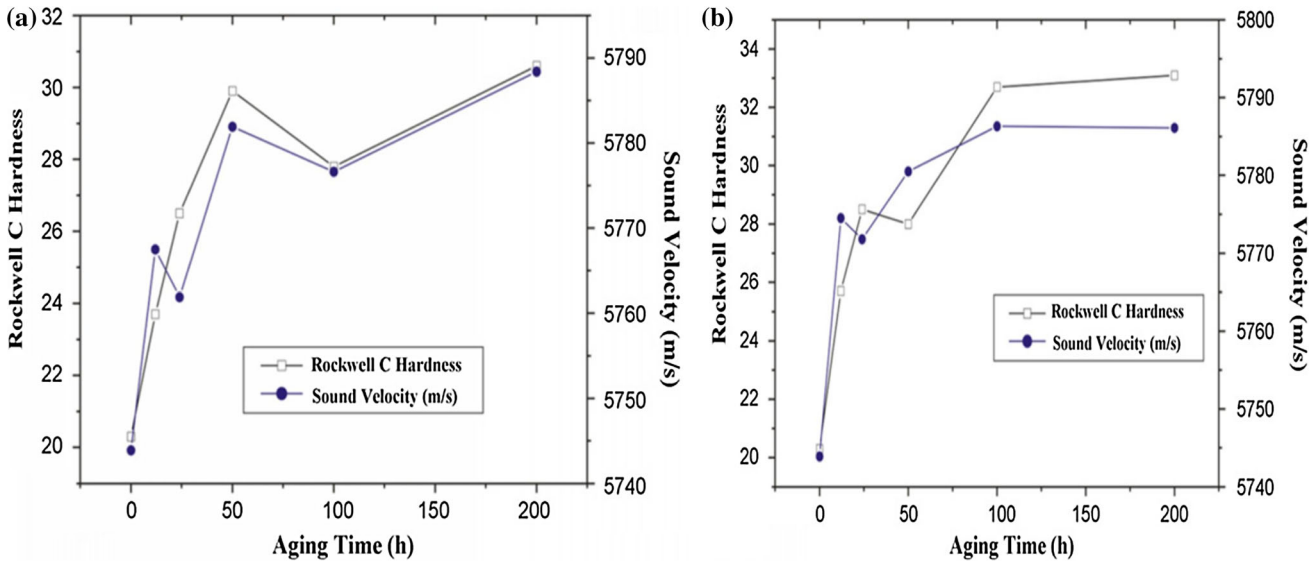

Fig. 17 Variation of velocity and hardness with aging time of UNS S31803 at: **a** 425 °C and **b** 475 °C [155]

chromium. However, the γ phase does not suffer transformation in this temperature range [158].

Ultrasonic measurements have shown the ability to characterize phase transformations by spinodal decomposition from 425 to 475 °C in the 2205 DSS [155–160]. Ultrasonic velocity is found to be increasing with the aging time, particularly at 475 °C (Fig. 17). Moreover, higher values of velocities at samples aged at 475 °C are correlated to the higher kinetics of phase decomposition at 475 °C [156]. Compositional variation generated by α'-phase decomposition during the long period of exposure to these temperatures increases the elastic modulus, provoking the increase of velocity values [156, 158, 159]. Other studies [155, 156] have found a direct relation between variations of the velocity and material hardness (Fig. 17) as reported by Badidi [67] and Korde and Kundu [68]. This similar relationship between velocity and hardness has been also found in duplex stainless steel JIS-SCS14A (CF8 M) by Tane et al. [161]. Two hardening stages in DSSs at both temperatures have been verified through ultrasonic velocity: one with ductile characteristic, and the other brittle in nature [155–158]. The first stage of hardening is characterized by formation of α' phase which is coherent to the matrix through spinodal decomposition mechanism and the second stage by the loose nature of coherency state with matrix and the coarsening of organized α' phase [153–155, 162]. In fact, α' phase or regions enriched in chromium are responsible for the variation in the rigidity of ferrite matrix and the increase in the ultrasonic velocity.

Ruiz et al. [163, 164] have investigated the kinetics of precipitation of aged specimen at 700 and 900 °C through the shear velocity and attenuation of longitudinal waves. The variation of attenuation coefficient reflects the microstructural variation that occurs during the aging treatments (Fig. 18). It can be seen that attenuation coefficient starts to decrease as aging time increases because of the early precipitation of sigma phase (Fig. 19). Two mechanisms have been reported to contribute to the decrease in the attenuation: (1) formation of new grain boundaries in the α-phase at shorter aging times, and (2) formation of new rounded grains of austenite and the reduction of the quantity of ferrite during the transformation $\delta \rightarrow \gamma + \sigma$ at longer aging times [163, 164]. It is clear that the attenuation coefficient changes only when the microstructure undergoes dramatic changes in the initial shape and the volume fraction of ferrite.

During the aging process, ferrite is transformed via $\delta \rightarrow \gamma + \sigma$, and the volume fraction of ferrite reduces, thus changing the initial texture of the steel which contributes to the variations in the fast mode of the shear velocity [163]. There are two different propagation modes of shear waves in a rolled aluminum plate; fast mode and slow mode associated to the polarization orientation with respect to the rolling direction. The direction parallel to the rolling direction corresponds to the fast principle axis, while the direction perpendicular to the rolling direction corresponds to the slow principle axis. However, fast mode is found to be more sensitive compared with the slow mode, Fig. 20 [163]. Velocity of the fast mode of shear wave is correlated to ferrite content and follows the similar trend of the ferrite content for both temperatures of 700 and 900 °C [161]. The main contribution to the increase in velocity is found to be the decrease in the lattice parameter of ferrite.

The main concern in the 650–900 °C range is that σ-phase begins to precipitate at relatively short aging

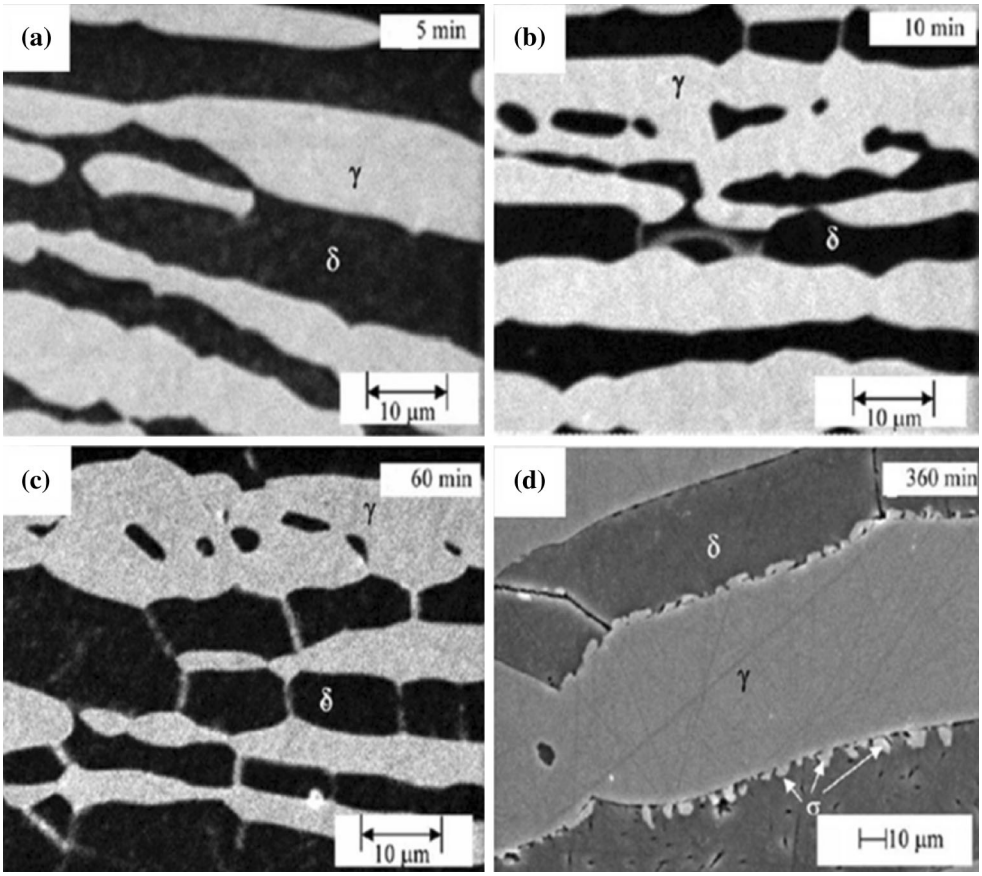

Fig. 18 SEM micrographs of the **a** 2205 DSS microstructure, **b** ferrite and austenite phases, **c** gradual formation of grain boundaries, and **d** sigma-phase precipitation [163]

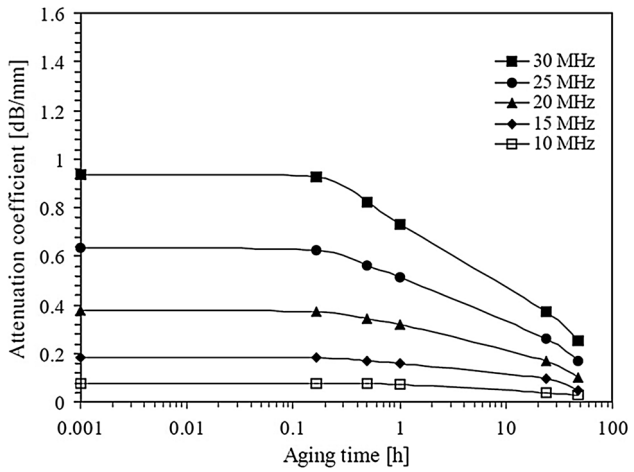

Fig. 19 Variations of the attenuation coefficient with aging times for 2205 DSS at 700 °C [164]

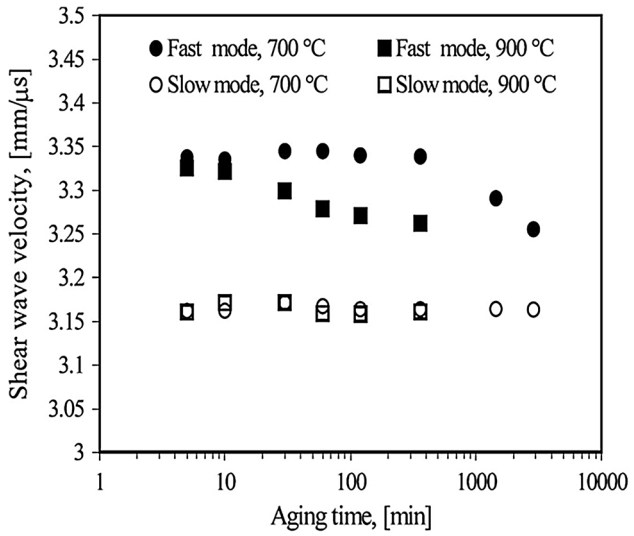

Fig. 20 Variations of shear wave velocity with aging time for 2205 DSS at 700 and 900 °C [163]

times, e.g., less than 30 min at 700 °C [163], and according to the literature, the fraction of sigma phase is too small to be detected even by destructive methods [163, 164]. No study has shown sufficient sensitivity of linear ultrasonic methods to detect changes during this early stage of thermal degradation (for the time up to 30 min after aging) due to the fast formation kinetics of σ phase. For example, in

the work by Ruiz et al. [163, 164], shear wave velocity measurement has shown no significant variations in the shear velocity and ferrite content at early aging times where the materials' properties are already degraded. Ruiz et al. [164] have introduced a nonlinear ultrasonic measurement for detection of precipitates at early stages of aging in 2205 DSS. Interestingly, nonlinearity parameter is found to be more sensitive than the velocity and attenuation measurements to the precipitation of σ and χ phases during the early stages of the aging treatments. The changes in the nonlinear parameter at short aging times have been correlated to the precipitation of σ- phase on grain boundaries during the aging treatment. It is also observed that the hardness measurements exhibits a very similar trend to the measured nonlinearity, which confirmed that the changes in nonlinearity were caused, at least during the early stage of aging, by the precipitation of sigma phase [163].

Nonlinear ultrasonic measurements have been shown to be much more sensitive than the conventional linear measurements in some cases such as structural changes and assessment of degradation of mechanical properties [12, 165]. The theory and principle of nonlinear ultrasonic were described by Viswanath et al. [12] and Jhang [165]. In nonlinear ultrasonic measurements, high-amplitude ultrasonic waves having a particular frequency are introduced into the material, causing generation of the harmonics as a result of interaction of ultrasonic waves with lattice discontinuities, such as cracks, interfaces, and voids. The amplitudes of these harmonics can be used to characterize the degradation of mechanical properties of material. Nonlinearity parameter, β, defined as the ratio of amplitude of the second harmonic to that of square of the fundamental amplitude, is principally associated to the dislocation density or arrangement, residual stress in the material, as well as precipitate–matrix coherency strains [12]. In general, nonlinear ultrasonic measurements primarily have been employed to characterize fatigue damage, precipitation behavior, and tensile deformation in various materials. Jhang [165] has reviewed overall progress in nonlinear ultrasonic measurements for characterization of micro-damages in solid material with state-of-the-art technologies.

The higher sensitivity of the nonlinear measurements to the embrittlement is demonstrated in Fig. 21 where the velocity and attenuation measurements have shown no changes in the early stages of aging. Figure 21 shows three distinctive stages of changes relative to the acoustic nonlinearity parameters or normalized second harmonic amplitude. The initial large change in the measured acoustic nonlinearity parameter is related to the precipitation of σ and χ phases as they start to precipitate on grain boundaries at short aging-treatment times [163]. The similar effect of second-phase precipitates on the nonlinear

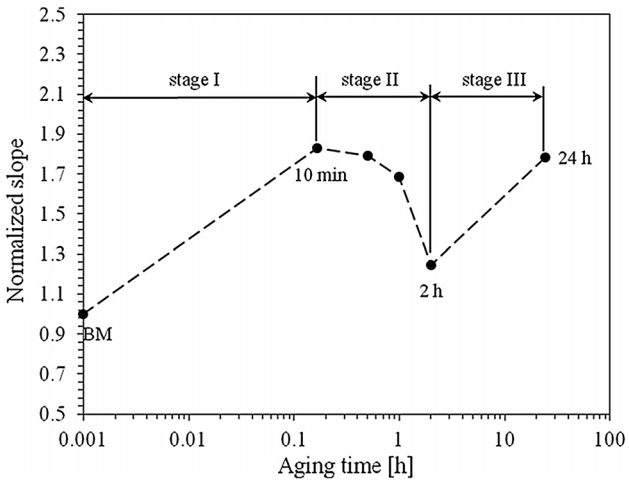

Fig. 21 Normalized second harmonic amplitude versus the aging time at 700 °C in 2205 DSS [164]

parameter has also been investigated wherein the nonlinear parameter in some cases linearly increases as the volume fraction of second phase increases [166, 167].

Thus, it may be concluded that ultrasonic measurements are capable of following-up the kinetics of phase transformation by spinodal decomposition and by detecting the hardening stages that occurred during phase transformation of DSSs. Despite the sensitivity of linear ultrasonic measurement to the transformation phases, nonlinear parameter can be used for characterization of early ferrite transformation of DSSs particularly at low aging times which is of primary importance from the point of view of thermomechanical stability and the beneficial effects of the duplex phase.

Measurement of degree of sensitization (DoS)

Stainless steels and aluminum alloys exposed to aggressive environment suffer a highly undesirable phenomenon known as sensitization which influences the mechanical and chemical properties of those materials. Sensitization is usually attributed to the gradual precipitation of secondary phases and formation of carbides at grain boundaries as well as the depletion of the adjacent area of alloying element, thereby making the material susceptible to corrosion particularly to intergranular corrosion (IGC) [168, 169].

Stella et al. [170] have found the increase in the attenuation coefficients with the increasing sensitization time in AISI 304 stainless steel. The increase in the attenuation coefficients is attributed to the quasi-continuous distribution and possible coalescence of the chromium carbide along the grain boundaries during the sensitization treatment, Fig. 22. Details of the grain boundary in the steel AISI 304 at different sensitization times are shown in Fig. 23. Although the modification of grain size along the

precipitated chromium carbides is expected, it is demonstrated that when sensitization phenomena are originated from the heat treatment, attenuation is not decided by scattering caused by grain size variation.

Ultrasonic velocity measurements do not provide significant information on the microstructural variations during the sensitization treatments in austenitic steels [170]. The ultrasonic velocity is associated to the volume fraction of each phase in a multiphase compound. The ultrasonic velocity of the compound (V) can be calculated from the formula $V = \sum f_i V_i$ where f_i is the volumetric fraction of each present phase, and V_i is the wave velocity in each phase [88, 170, 171]. Because of the extremely low volumetric fraction of the precipitated carbides at grain boundaries, velocity measurements are not applicable in the characterization of DoS.

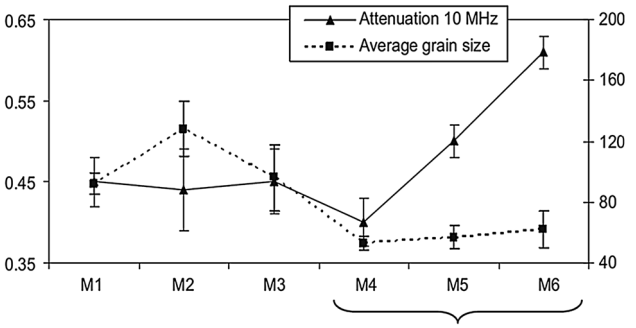

Fig. 22 Variation of the attenuation at 10 MHz with the average grain size in AISI 304 stainless steel [170]

The amplitude of the each peak in the power spectra at specific frequencies is strongly affected by the DoS as shown in Fig. 24 and reported by Stella et al. [170]. The power spectra for the AISI 304 steels sensitized at 800 °C for 10 h obtained by 5 and 7.5 MHz transducers are shown in Fig. 24. Power spectra at frequency ranges are almost independent of the heat treatment, while the peak height of each spectrum is affected by the DoS. It has been found that the power density at the main frequency increases as the sensitization time increases. However, the increases in the power spectra at longer aging times are in agreement with the increasing attenuation (Fig. 22). The increase in the main peak height of each spectrum for longer sensitization times is associated to the higher homogenization of the materials as a consequence of the long exposure at high temperature, and not the precipitation or the coalescence of carbides at grain boundary.

In the work by Li et al. [171], it is found that shear wave velocities of the same frequency are more sensitive to DoS, as longitudinal wave velocity measurement is independent of the sensitization of AA5083 aluminum alloy (Fig. 25). The longitudinal velocity is found to be almost constant mainly because of the similar values of velocity for both β-phase and α-phase. As velocity in a multiphase

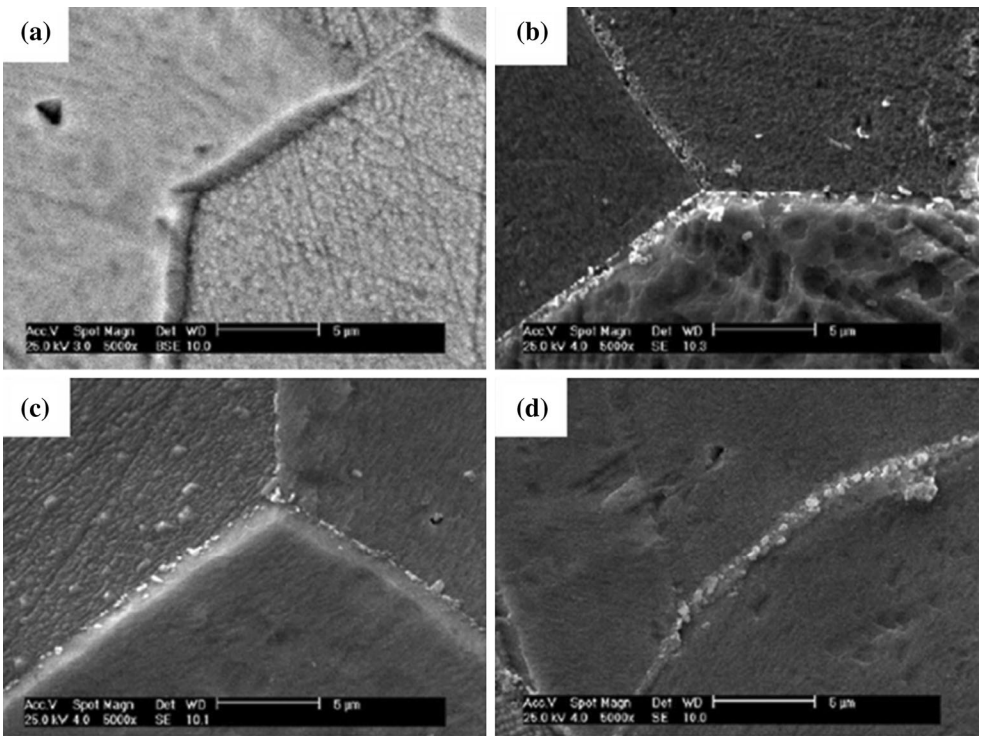

Fig. 23 Details of the grain boundary in the steel AISI 304 of original condition (**a**), sensitization times of 2 h (**b**), 6 h (**c**), and 10 h (**d**) [170]

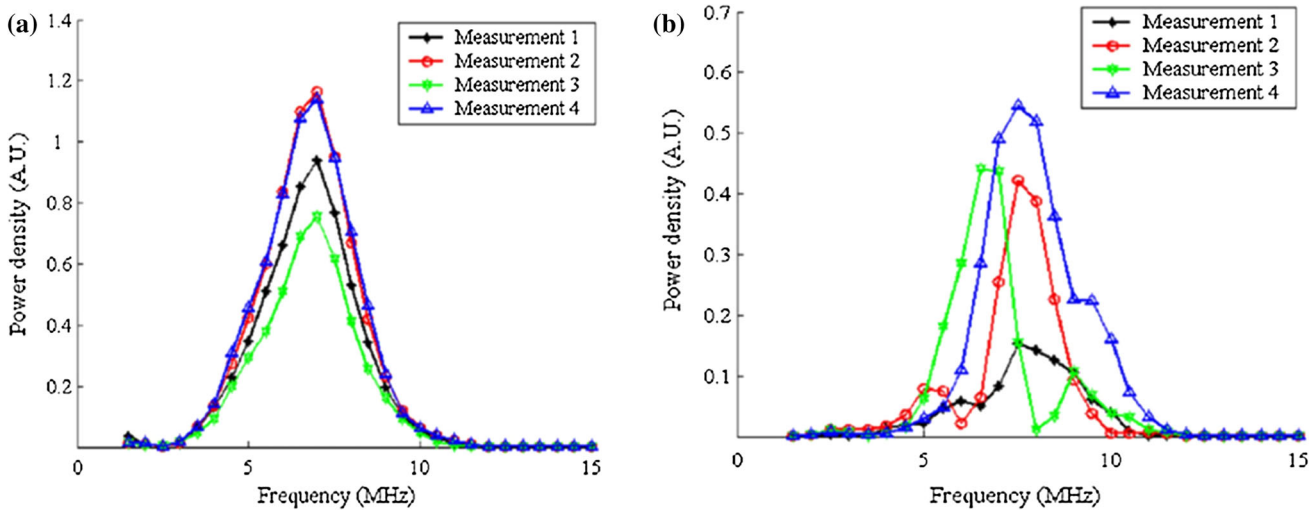

Fig. 24 Power spectra obtained from (**a**) 5 MHz transducer and (**b**) 7.5 MHz transducer in AISI 304 stainless steel at 800 °C for 10 h [170]

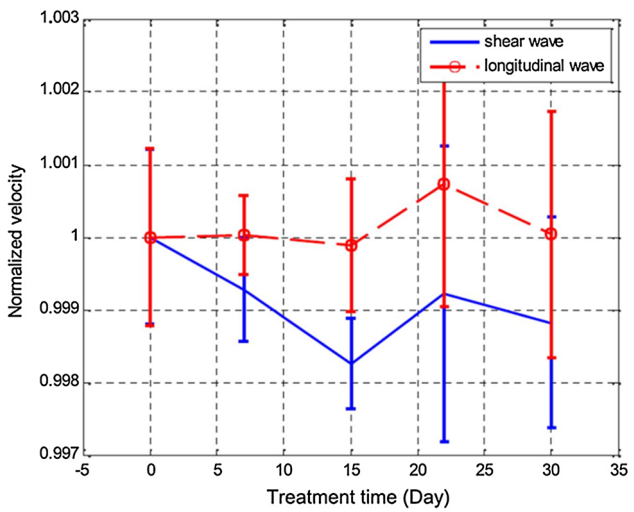

Fig. 25 The ultrasonic velocity variations with sensitization times at 100 °C for AA5083 aluminum alloy [171]

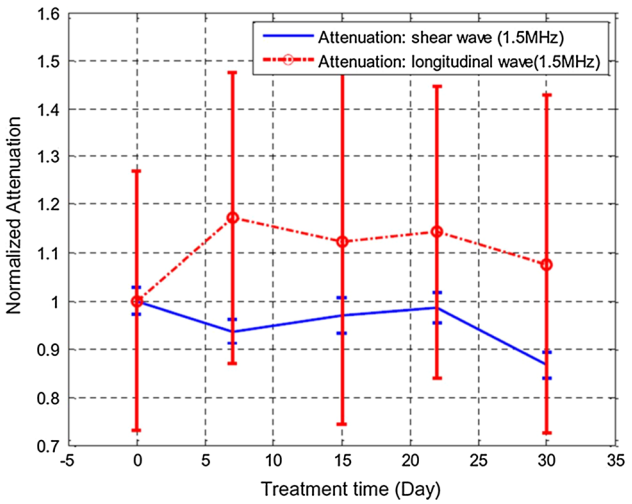

Fig. 26 The ultrasonic longitudinal and shear attenuation variations with sensitization for AA5083 at 100 °C at different times as obtained by 1.5 MHz transducer [171]

component is related to the volume fraction of each phase, the decrease in shear velocity with the sensitization time could be attributed to the lower shear velocity value of β-phase than that of α-phase.

As sensitization proceeds, the precipitation of β-phase increases, while grain size variation is not appreciable. These microstructural changes reveal that variations of the attenuation with the sensitization times are because of the precipitation of the β-phase along the grain boundaries. The variations in the grain boundary condition facilitate the propagation of shear and longitudinal waves through the grain boundaries [171]. It is found that shear attenuation is more sensitive to the sensitization than longitudinal attenuation (Fig. 26). The shear waves have larger wavelength than the longitudinal ones at the same frequency and are more easily scattered back as they propagate through the grain boundaries. As can be seen in Fig. 26, shear attenuations show lower values than longitudinal attenuations due to the fact that attenuation is smaller for the waves with a smaller wavelength as reported by Hirsekorn [104]. Besides, higher-frequency shear wave velocity and attenuation are found to be more sensitive to the DoS [171]. However, the employment of higher frequencies is impractical in the field of coarse-grained materials like austenitic steels because of the high attenuation exhibited by these materials.

In conclusion, a good correlation has been established between DoS and the shear wave velocity and attenuation,

providing easier characterization of DoS in aluminum and stainless steels. The changes in the attenuation and velocity of ultrasonic waves are linked to microstructural variations as a result of precipitation of secondary phases. The sensitization treatment has little effect on the longitudinal wave velocity, whereas the shear waves have shown a significant sensitivity to sensitization. Further, assessments of both the attenuations and amplitudes of the main peaks on the power spectra provide a predictive criterion in order to estimate any microstructural change caused by the sensitization.

Conclusions

This paper has reviewed the established ultrasonic evaluation technique as the most widely used nondestructive forms of testing. The aim of the review was to provide a better insight into the interaction of ultrasonic wave with microstructural features of ferrous and nonferrous metal alloys in practical situations. The specific focus has been specialized to comprehensive assessment of the variation in microstructures and mechanical properties induced by the heat-treatment processes, and in-service condition or elevated temperatures. It has been concluded from the results that ultrasonic techniques are correlated with variations of microstructure, formation of secondary phases, or precipitates which frequently occur during the heat-treatment process. The overwhelming majority of studies indicated that ultrasonic parameters variations are a function of structural state and changes in the intrinsic properties of materials like elastic module, which are mainly associated with the compositional variations of phases involved and formation of different precipitates due to heat-treatment processes. It is believed that ultrasonic evaluation techniques could be reliably used in the future to evaluate microstructural variations and the consequent mechanical properties of materials so far away, keeping pace with the advancement of the ultrasonic equipment and methodologies.

Acknowledgements The authors are most grateful to the Universiti Putra Malaysia for the financial support extended to this research work. The first author would like to thank F. Lesani for her assistance in the manuscript preparation.

References

1. Gür CH (2013) Characterization of steel microstructures by magnetic barkhausen noise technique. Nondestruct Test Mater Struc 6:499–504
2. Raj B (1996) A perspective on materials characterization for technology advancement and industrial growth: emphasis on non-destructive evaluation. Bull Mater Sci 19:839–855
3. Kaplan M, Gür CH, Erdogan M (2007) Characterization of dual-phase steels using magnetic barkhausen noise technique. J Nondestruct Eval 26:79–87
4. Singh R (2012) Heat treatment of steels. In: Singh RR (ed) Applied welding engineering: processes, codes, and standards. Elsevier Ltd, Amsterdam, pp 95–108
5. Gestwa W, Przylecka M, MacKenzie DM, Pye D, Totten GE (2004) Heat treatment. In: Gale WF, Totemeier TC (eds) Smithells metals reference book, 8th edn. Elsevier Ltd, Amsterdam, pp 1–83
6. Raj B, Jayakumar T (1997) NDE methodologies for characterization of defects, stresses and microstructures in pressure vessels and pipe. Int J Press Vessel Piping 73:133–146
7. Freitas V, Albuquerque V, Silva E, Silva A, Tavares JMRS (2010) Nondestructive characterization of microstructures and determination of elastic properties in plain carbon steel using ultrasonic measurements. Mater Sci Eng A 527:4431–4437
8. Nanekar PP, Shah BK (2003) Characterization of material properties by ultrasonic. BARC Newsl 249:25–38
9. García-Martín J, Gómez-Gil J, Vázquez-Sánchez E (2011) Non-destructive techniques based on eddy current testing. Sensors 11:2525–2565
10. Manjula K, Vijayarekh K, Venkatraman B, Karthik D (2012) Ultrasonic time of flight diffraction technique for weld defects: a review. J Appl Sci Eng Tech 4:5525–5533
11. Normando PG, Moura EP, Souza JA, Tavares SM, Padovese LR (2010) Ultrasound, eddy current and magnetic Barkhausen noise as tools for sigma phase detection on a UNS S31803 duplex stainless. Mater Sci Eng A 527:2886–2891
12. Viswanath A, Rao BPC, Mahadevan S, Parameswaran P, Jayakumara T, Raj B (2011) Nondestructive assessment of tensile properties of cold worked AISI type 304 stainless steel using nonlinear ultrasonic technique. J Mater Process Tech 211:538–544
13. Muthmari S, Singh A (2011) Review of various ultrasonic techniques employed in modern industries. Int J Eng Sci Tech 3:3078–3085
14. Zergoug M, Kamel G, Boucherou N (2008) Mechanical stress analysis by eddy current method. J Am Sci 4:1–6
15. Konoplyuk S (2010) Estimation of pearlite fraction in ductile cast irons by eddy current method. NDT E Int 43:360–364
16. Rosen M, Horowitz E, Swartzendruber L, Fick S, Mehrabian R (1982) The aging process in aluminum alloy 2024 studied by means of eddy currents. Mater Sci Eng 53:191–198
17. Sasi B, Rao BPC, Jayakumar T, Raj B (2010) Characterisation of solution annealed VT-4 titanium alloy using eddy current based electrical resistivity measurements. Trans Indian Inst Met 63:773–777
18. Auld BA, Moulder JC (1999) Review of advances in quantitative Eddy Current nondestructive evaluation. J Nondestruct Eval 18:3–35
19. Santa-aho S, Vippola M, Sorsa A, Leiviskä K, Lindgren M, Lepistö T (2012) Utilization of barkhausen noise magnetizing sweeps for case-depth detection from hardened steel. NDT E Int 52:95–102
20. Tomita Y, Hashimoto K, Osawa N (1996) Nondestructive estimation of fatigue damage for steel by Barkhausen noise analysis. NDT E Int 29:275–280
21. Rao BPC, Jaykumar T, Raj B, Arnold W (2001) Nondestructive characterization of martensite in AISI type 304 stainless steel using Squid and MBN methods. J Nondestruct Eval 21:38–43
22. Franco FA, González MFR, Campos MF, Padovese LR (2013) Relation between magnetic barkhausen noise and hardness for jominy quench tests in SAE 4140 and 6150 steels. J Nondestruct Eval 32:93–103

23. Zhu Y, Tian GY, Lu RS, Zhang H (2011) A review of optical NDT technologies. Sensors 11:7773–7798
24. Awal MA (1995) Low frequency acoustic microscopy for material characterization. PhD Dissertation, University of Arizona
25. Luangvilai K (2007) Attenuation of ultrasonic lamb waves with applications to material characterization and condition Monitoring. PhD Dissertation, Georgia institute of technology
26. Vogt TK (2002) Determination of material properties using guided waves. PhD Dissertation, Imperical college of science, technology and medicine
27. Pandey DK, Pandey S (2010) Ultrasonics: A Technique of Material Characterization. In: Dissanayake DW (ed), Acoustic waves. Sciyo, Croatia, pp 397–430
28. Ewert U, Jaenisch GR, Osterloh K, Zscherpel U (2011) Performance control: nondestructive testing and reliability evaluation. In: Czichos H, Saito T, Smith (eds) Springer handbook of metrology and testing, 2nd edn. Springer, Berlin, pp 887–972
29. Hendee WR, Ritenour ER (2002) Medical imaging physics, 4th edn. Wiley-Liss Inc, London
30. Hirao M, Ogi H (2003) EMATs for science and industry noncontacting ultrasonic measurements. Kluwer Academic Publishers, Dordrecht
31. Badidi Bouda A, Lebaili S, Benchaala A (2003) Grain size influence on ultrasonic velocities and attenuation. NDT E Int 36:1–5
32. Krautkramer J, Krautkramer H (1983) Ultrasonic testing materials, 2nd edn. Springer, New York
33. Hellier CJ (2003) Handbook of nondestructive evaluation. Mc Graw-Hill, New York
34. Han YK, Thompson RB (1997) Ultrasonic backscattering in duplex microstructures: theory and application to titanium alloys. Metall Mater Trans A 28:91–104
35. Lobkis OI, Yang L, Li J, Rokhlin SI (2012) Ultrasonic backscattering in polycrystals with elongated single phase and duplex microstructures. Ultrasonics 52:694–705
36. Mora EP, Normando PG, Gonçalvs LL, Kruger SE (2012) Characterization of cast iron microstructure through fluctuation and fractal analyses of ultrasonic backscattered signals combined with classification techniques. J Nondestruc Eval 31:90–98
37. Kruger SE, Rebello JMA, De Camargo PC (1999) Hydrogen damage detection by ultrasonic spectral analysis. NDT E Int 32:275–281
38. Cong S, Gang T (2012) Ultrasonic thickness measurement for aluminum alloy irregular surface parts based on spectral analysis. J Trans Nonferr Metal Soc 22:323–328
39. Kumar A, Jaykumar T, Palanichamy P, Raj B (1999) Influence of grain size on ultrasonic spectral parameters in AISI type 316 stainless steel. Scr Mater 40:333–340
40. Leviston D, Bridge B (1988) Evaluation of the subsurface microstructure of quenched and tempered carbon steel by ultrasonic backscatter. NDT Int 21:17–25
41. Palanichamy P, Joseph A, Jayakumar T, Raj B (1995) Ultrasonic velocity measurements for estimation of grain size in austenitic stainless steel. NDT E Int 28:179–185
42. Fowler KA, Elfbaum GM, Smith KA, Nelligan TJ (1997) Theory and application of precision ultrasonic thickness gaging. Panametrics Application Notes. http://www.ndt.net/article/wt1097/panam/panam.htm
43. Papadakis EP (1972) Absolute accuracy of the pulse-echo overlap method and pulse-superposition method for ultrasonic velocity. J Acoust Soc Am 52:843–846
44. Papadakis EP (1967) Ultrasonic phase velocity by pulse-echo overlap method incorporating diffraction phase corrections. J Acoust Soc Am 42:1045–1051
45. Edmonds PD, Dunn F (1981) Physical description of ultrasonic fields. In: Edmonds PD (ed) Methods of experimental physics: ultrasonics. Academic Press, New York
46. Herzfeld KF, Litovitz TA (1959) Absorption and dispersion of ultrasonic waves. Academic Press, New York
47. Papadakis EP (1968) Ultrasonic attenuation caused by scattering in polycrystalline media. In: Mason W (ed) Physical Acoustics, IVB. Academic Press, New York, pp 269–328
48. Papadakis EP (1965) Revised grain-scattering formulas and tables. J Acoust Soc Am 37:703–710
49. Mason WP, McSkimmin HJ (1947) Attenuation and scattering of high frequency sound waves in metals and glasses. J Acous Soc Am 19:464–473
50. Mason WP, McSkimmin HJ (1948) Energy losses of sound waves in metals due to scattering and diffusion. J Appl Phys 19:940–946
51. Stanke FE, Kino GS (1984) A unified theory for elastic wave propagation in polycrystalline materials. J Acous Soc Am 75:665–681
52. Weaver RL (1990) Diffusivity of ultrasound in polycrystals. J Mech Phys Solids 38:55–86
53. Mason WP (1958) Physical acoustics and properties of solids. Van Nostrand, Princeton, NJ
54. Truell R, Elbaum C, Chick BB (1969) Ultrasonic methods in solid state physics. Academic Press, New York
55. Papadakis EP (1990) The measurement of ultrasonic velocity. In: Thurston RN, Pierce AD (eds) Physical acoustics, vol XIX. Academic Press, Boston, pp 81–106
56. Papadakis EP (1990) The measurement of ultrasonic velocity. In: Thurston RN, Pierce AD (eds) Physical acoustics, vol XIX. Academic Press, Boston, pp 107–155
57. Papadakis EP (1976) Ultrasonic velocity and attenuation: Measurement methods and scientific and industrial applications. In: Mason WP, Thurston RN (eds) Physical acoustics: principles and methods, vol XII. Academic Press, New York, pp 277–374
58. Papadakis EP (1981) Physical acoustics: principles and methods. Academic Press, New York, pp 269–370
59. Papadakis EP (1964) Ultrasonic attenuation and velocity in three transformation products in steel. J Acoust Soc Am 35:1474–1481
60. Papadakis EP (1970) Ultrasonic attenuation and velocity in AISI/SAE 52100 steel quenched from various temperatures. Metall Trans 1:1053–1057
61. Kidd TH, Zhuang S, Ravichandran G (2007) An in situ ultrasonic technique for simultaneous measurement of longitudinal and shear wave speeds in solids. Exp Mech 47:753–759
62. Kim SA, Johnson LW (2007) Elastic constants and internal friction of martensitic steel, ferritic-pearlitic steel, and α-iron. Mater Sci Eng A 452–453:633–639
63. Kumar A, Jaykumar T, Raj B (2006) Influence of precipitation of intermetallics on Young's modulus in nickel and zirconium base alloy. Philos Mag Let 86:579–587
64. Dubois M, Militzer M, Moreau A, Bussière JF (2000) A new technique for the quantitative real-time monitoring of austenite grain growth in steel. Scr Mater 42:867–874
65. Lévesque D, Kruger SE, Lamouche G, Kolarik R, Jeskey G, Choquet M, Monchalin JP (2006) Thickness and grain size monitoring in seamless tube making process using laser-ultrasonics. In: Proceeding of advances in signal processing for nondestructive evaluation of materials, pp 51–56
66. Botvina LR, Fradkin LJ, Bridge B (2000) A new method for assessing the mean grain size of polycrystalline materials using ultrasonic NDE. J Mater Sci 35:4673–4683. doi:10.1023/A:1004890604013
67. Badidi Bouda A, Benchaala A, Alem K (2000) Ultrasonic characterization of materials hardness. Ultrasonics 38:224–227

68. Korde N, Kundu T (2013) Material hardness and aging measurement using guided ultrasonic waves. Ultrasonics 53:506–510
69. Aghaie-Khafri M, Honarvar F, Zanganeh S (2012) Characterization of grain size and yield strength in AISI 301 stainless steel using ultrasonic attenuation measurements. J Nondestruct Eval 31:191–196
70. Kwon SI, Hong ST, Choo WY (2000) Ultrasonic nondestructive evaluation of microstructure and strength of carbon steels. J Mater Sci let 19:1453–1456
71. Smith RL (1983) Ultrasonic attenuation, microstructure and ductile to brittle transition temperature in Fe–C alloys. J Mater Eval 41:219–222
72. Vary A (1998) Concepts for interrelating ultrasonic attenuation, microstructure and fracture toughness in polycrystalline solids. J Mater Eval 46:642–649
73. Generazio ER (1998) Ultrasonic attenuation measurements to determine onset, degree and completion of recrystallization. J Mater Eval 46:1198–1203
74. Vasudevan M, Palanichami P (2002) Characterization of microstructural changes during annealing of cold worked austenitic stainless steel using ultrasonic velocity measurements and correlation with mechanical Properties. J Mater Eng Perform 11:169–179
75. Baqeri R, Honarvar F, Mehdizad R (2012) Case depth profile measurement of hardened components using ultrasonic backscattering method. Proceeding of 18th world conference on nondestructive testing. Durban, South Africa, pp 16–20
76. Weston-Bartholomew W (1979) Use of ultrasonic goniometer to measure depth of case hardening. Int Adv Nondestruct Test 6:111–123
77. Meyendorf GH, Rösner H, Kram V, Sathish S (2002) Thermoacoustic fatigue characterization. Ultrasonics 40:427–434
78. Cantrell HJ, Yost TW (2001) Nonlinear ultrasonic characterization of fatigue microstructures. Int J Fatigue 23:487–490
79. Nagy BP (1998) Fatigue damage assessment by nonlinear materials characterization. Ultrasonics 36:375–381
80. Ohtani T, Nishiyama K, Yoshikawa S, Ogi H, Hirao M (2006) Ultrasonic attenuation and microstructural evolution throughout tension–compression fatigue of a low-carbon steel. Mater Sci Eng A 442:466–470
81. Jaykumar T, Mukhopadhyay CK (2010) Non-destructive evaluation techniques for assessment of creep and fatigue damage in materials and components. Trans Indian Inst Met 63:301–311
82. Yassen Y, Ismail MP, Jemain AA, Daud AR (2011) Reliability of ultrasonic measurement of thickness loss caused by corrosion. Insight Nondestruct Test Cond Monitor 53:658–663
83. Birring AS, Bartlett ML, Kawano K (1998) Ultrasonic detection of hydrogen attack in steels. Corrosion 45:259–263
84. Javadi Y, Afzali O, Raeisi HM, Najafabadi AM (2013) Nondestructive evaluation of welding residual stresses in dissimilar welded pipes. J Nondestruct Eval 32:177–187
85. Nikitina NY, Ostrovsky LA (1998) An ultrasonic method for measuring stresses in engineering materials. Ultrasonics 35:605–610
86. Roy AK, Bandyopadhyay S, Suresh SB, Wells D (2006) Comparison of residual stress in martensitic alloys by nondestructive techniques. Mater Sci Eng A 419:372–380
87. Kop TA, Sietsma J, Van Der Zwaag S (2001) Dilatometric analysis of phase transformations in hypo-eutectoid steels. J Mater Sci 36:519–526. doi:10.1023/A:1004805402404
88. Leslie WC, Hornbogen E (1996) Physical metallurgy of steels. In: Cahn RW, Haasent P (eds) Physical metallurgy, 4th edn. Elsevier Science BV, NY
89. Kruger SE, Damm BE (2006) Monitoring austenite decomposition by ultrasonic velocity. J Mater Sci Eng A 425:238–243
90. Scruby CB, Moss BC (1993) Non-contact ultrasonic measurements on steel at elevated temperatures. NDT E Int 26:177–188
91. Dubois M, Moreau A, Bussière JF (2001) Ultrasonic velocity measurements during phase transformations in steels using laser ultrasonics. J Appl Phys 89:6487–6495
92. Dubois M, Moreau A, Militzer M, Bussière JF (1998) Laser ultrasonic monitoring of phase transformation in steels. Scripta Mater 39:735–741
93. Lamouche G, Bolognini S, Kruger SE (2004) Influence of steel heat treatment on ultrasonic absorption measured by laser ultrasonic. Mater Sci Eng A 370:401–406
94. Kruger SE, Bolognini S, Lamouche G (2003) Laser ultrasonics monitoring of LC steel absorption during annealing. In: Proceedings of the 11th international symposium on non-destructive characterization of materials, Germany, pp 33–38
95. Prasad R, Kumar S (1991) An investigation into the ultrasonic behaviour of cast and heat-treated structures in steel. Br J Nondestruct Test 33:506–508
96. Murav'ev VV (1989) Interrelationship of the velocity of an ultrasonic wave in steels and their heat cycles. Soviet J NDT 25:135–137
97. Pandey JC (2011) Study of recrystallization in interstitial free (IF) steel by ultrasonic techniques. Mater Manufact Process 26:147–153
98. Gür HC, Tuncer OB (2005) Characterization of microstructural phases of steels by sound velocity measurement. Mater Charact 55:160–166
99. Gür HC, Çam I (2007) Comparison of magnetic Barkhausen noise and ultrasonic velocity measurements for microstructure evaluation of SAE 1040 and SAE 4140 steels. Mater Charact 58:447–454
100. Grayali N, Shyne JC (1985) Effect of microstructure and prior austenite grain size on acoustic velocity and attenuation in steel, review of progress in NDE. Plenum Press, New York, pp 927–936
101. Albuquerque VHC, Melo TAA, De Oliveira DF, Gomes RM, Tavares JMRS (2010) Evaluation of grain refiners influence on the mechanical properties in a CuAlBe shape memory alloy by ultrasonic and mechanical tensile testing. Mater Des 31:3275–3281
102. Gür CH, Keleş Y (2003) Ultrasonic characterization of hot-rolled and heat-treated plain carbon steels. Insight Br J NDT 45:615–620
103. Hirsekorn S (1982) The scattering of ultrasonic waves by polycrystals. J Acoust Soc Am 72:1021–1031
104. Hirsekorn S (1983) The scattering of ultrasonic waves by polycrystals. II. Shear waves. J Acoust Soc Am 73:1160–1163
105. Vasudevan M, Palanichami P, Venkadesan S (1994) A novel technique for characterizing annealing behavior. Scr Metall Mater 30:1479–1483
106. Prasad R, Kumar S (1994) Study of the influence of deformation and thermal treatment on the ultrasonic behavior of steel. J Mater Process Tech 42:51–59
107. Kumar A, Laha K, Jaykumar T, Rao KBS, Raj B (2002) Comprehensive microstructural characterization in modified 9Cr-1Mo ferritic steel by ultrasonic measurements. Metall Mater Trans A 33:1617–1626
108. Kumar A, Choudhary BK, Laha K, Jayakumar T, Rao KBS, Raj B (2003) Characterization of microstructure in 9% chromium ferritic steels using ultrasonic measurements. Trans Indian Inst Met 56:483–497
109. Kumar A, Choudharby K, Jaykumar T, Rao KBS, Raj B (2000) Influence of thermal ageing and creep on ultrasonic velocity in 9Cr-1Mo ferritic steel. Trans Indian Inst Met 53:341–345
110. Mc. Intrie P (1991) Non-destructive testing handbook: ultrasonic testing. American Society for Non-Destructive Testing, USA

111. Vary A (1980) Ultrasonic measurement of material properties. In: Sharpe RS (ed) Research techniques in non-destructive testing. Academic Press, New York, pp 159–204
112. Papadakis EP (1984) Physical acoustics and microstructure of iron alloys. Inter Met Rev 29:1–24
113. Kruger SE, Rebello JMA (1998) Ultrasonic backscattering formulation applied to cast iron characterization. http://www.ndt.net/article/ecndt98/material/171/171.htm
114. Klimman R, Webster GR, Marsh FJ, Stepherson ET (1980) Ultrasonic prediction of grain size, strength, and toughness in plain carbon steel. Mat Eval 38:26–32
115. Matos JMO, de Moura EP, Krüger SE, Rebello JMA (2004) Rescaled range analysis and detrended fluctuation analysis study of cast irons ultrasonic backscattered signals. Chaos, Solitons Fractals 19:55–60
116. Ramuhalli P, Good MS, Diaz AA, Anderson MT, Watson BE, Peters TJ, Dixit M, Bond LJ (2009) Ultrasonic characterization of cast austenitic stainless steel microstructure: discrimination between equiaxed and columnar-grain material—an interim study, Technical reported of the U.S. Nuclear Regulatory
117. Anderson MT, Bond LJ, Diaz AA, Good MS, Harris RV, Mathews R, Ramuhalli P, Roberts KC (2010) In-situ characterization of cast stainless steel microstructures. In: Proceedings of the 8th international conference on NDE in relation to structural integrity for nuclear and pressurised components, Germany, pp 1036–1045
118. Hsu CH, Teng HY, Chen YJ (2004) Relationship between ultrasonic characteristics and mechanical properties of tempered martensitic stainless steel. J Mater Eng Perform 13:593–599
119. Vijayalakshmi K, Muthupandi V, Jayachitra R (2011) Influence of heat treatment on the microstructure, ultrasonic attenuation and hardness of SAF 2205 duplex stainless steel. Mater Sci Eng A 529:447–451
120. Jayachitra R, Muthupandi V, Vijayalakshmi K (2012) Characterization of duplex stainless steel heat-treated at 1300 °C. Int J Sci Res Public 2:1–6
121. Kumar A, Jayakumar T, Raj B, Ray KK (2003) Correlation between ultrasonic shear wave velocity and Poisson's ratio for isotropic solid materials. Acta Mater 51:2417–2426
122. Ringer SP, Hono K (2000) Microstructural evolution and age hardening in aluminium alloys: atom probe field-ion microscopy and transmission electron microscopy studies. Mater Charact 44:101–131
123. Chakrabarti DJ, Laughlin DE (2004) Phase relations and precipitation in Al–Mg–Si alloys with Cu additions. Prog Mater Sci 49:389–410
124. Polmear IJ (2005) Physical metallurgy of aluminium alloys, 4th edn. Elsevier Ltd, Amsterdam
125. Gefen Y, Rosen M, Rosen A (1971) Aging phenomena in Duraluminum 2024 studied by resistometry and hardness. Mater Sci Eng 8:181–188
126. Tariq F, Naz N, Baloch R, Faisal A (2012) Characterization of material properties of 2xxx series Al-alloys by nondestructive testing techniques. J Nondestruct Eval 31:17–33
127. Gefen Y, Rosen M, Rosen A (1971) Behaviour of ultrasonic attenuation during aging of Duraluminum 2024. Mater Sci Eng 8:246–247
128. Muthu Kumaran S (2011) Evaluation of precipitation reaction in 2024 Al–Cu alloy through ultrasonic parameter. Mater Sci Eng A 528:4152–4158
129. Muthu Kumaran S, Priyadharsini N, Rajendran V, Jayakumar T, Palanichamy P, Shankar P, Raj B (2006) In situ high temperature ultrasonic evaluation for on-line characterization of fine scale precipitation reactions in 8090 Al–Li alloy. Mater Sci Eng A 435–436:29–39
130. Rajendran V, Muthu Kumaran S, Jayakumar T, Palanichamy P, Raj B (2005) Ultrasonic studies for microstructural characterization of AA8090 aluminium–lithium alloy. Mater Eval 63:837–842
131. Rosen M, Ives L, Ridder S, Biancaniello F, Mehrabian R (1985) Correlation between ultrasonic and hardness measurement in aged aluminum alloy 2024. Mater Sci Eng 74:1–10
132. Toozandehjani M, Mustapha F, Ismarrubie NZ, Ariffin MKA, Matori KA, Ostovan F, Lim WF (2014) Characterization of aging behavior of AA6061 aluminum alloy through destructive and ultrasonic non-destructive testing techniques. Trans Indian Inst Met. doi:10.1007/s12666-014-0486-4
133. Rosen M, Horowitz E, Fick S, Reno RC, Mehrabian R (1982) An investigation on the precipitation hardening process in aluminum alloy 2219 by means of sound wave velocity and ultrasonic attenuation. Mater Sci Eng 53:163–177
134. Murav'ev VV (1989) Effects of heat treatment on the speed of ultrasound in aluminum alloys. Soviet J Nondestruct Test 25:832–839
135. Gür CH, Yildiz I (2004) Non-destructive investigation on the effect of precipitation hardening on the impact toughness of 7020 Al–Zn–Mg alloy. Mater Sci Eng A 382:395–400
136. Gür CH, Yildiz I (2008) Utilization of non-destructive methods for determining the effect of age-hardening on impact toughness of 2024 Al–Cu–Mg alloy. J Nondestruct Eval 27:99–104
137. Gür CH, Yildiz I (2004) Determining the impact toughness of age hardened 2024 AL-alloy by nondestructive measurements. In: Proceeding of the 16th world conference on NDT, Montreal, Canada
138. Kumar A, Rajkumar KV, Jayakumar T, Raj B, Mishra B (2006) Ultrasonic measurements for in-service assessment of wrought Inconel 625 cracker tubes of heavy water plants. J Nuclear Mater 350:284–292
139. Albuqueque VHC, Silva CC, Normando PG, Moura EP, Tavares JMRS (2012) Thermal aging effects on the microstructure of Nb-bearing nickel based superalloy weld overlays using ultrasound techniques. Mater Des 36:337–347
140. Palanichamy P, Mathew MD, Latha S, Jaykumar T, Rao KBS, Mannan SL, Raj B (2001) Assessing microstructural changes in alloy 625 using ultrasonic waves and correlation with tensile properties. Scr Mater 45:1025–1030
141. Shah BK, Nanekar PP, Bandyopadhyay M (1996) Ultrasonic characterization of aging degradation during long term high temperature exposure in Nickel base alloy 625. In: Proceeding of 14th world conference on NDT, New Delhi, pp 2235–2238
142. Kumar A, Shankar V, Jaykumar T, Rao KBS, Raj B (2002) Correlation of microstructure and mechanical properties with ultrasonic velocity in the Ni-based superalloy Inconel 625. Philos Mag A 82:2529–2545
143. Kumar A, Shankar V, Jayakumar T, Rao, KBS, Raj B (2002) Effect of precipitates on the correlation of ultrasonic velocity with mechanical properties in Ni-based superalloy Inconel 625. In: Proceeding of European conference on nondestructive testing, Spain
144. Nishara Begum A, Rajendran V, Jayakumar T, Palanichamy P, Priyadharsini N, Aravindan S, Raj B (2007) On-line ultrasonic velocity measurements for characterization of microstructural evaluation during thermal aging of β-quenched zircaloy-2. Mater Charact 58:563–570
145. Gopalan P, Rajaraman R, Amarendra G, Sundar CS, Viswanathan B, Jayakumar T, Palanichamy P, Raj B (2005) Characterisation of β-quenched and thermally aged Zircaloy-2 by positron annihilation, hardness and ultrasonic velocity measurements. J Nuclear Mater 345:162–166
146. Jayakumar T, Palanichamy P, Raj B (1998) Detection of hard intermetallics in b-quenched and thermally aged Zircaloy-2 using ultrasonic measurements. J Nuclear Mater 255:243–249
147. Shankar V, Rao KBS, Mannan SL (2001) Microstructure and mechanical properties of Inconel 625 superalloy. J Nuclear Mater 288:222–232

148. Murthy GVS, Ghosh S, Das M, Ghosh RN (2008) Correlation between ultrasonic velocity and indentation-based mechanical properties with microstructure in Nimonic 263. Mater Sci Eng, A 488:398–405
149. Murthy GVS, Sridhar G, Kumar A, Jaykumar T (2009) Characterization of intermetallic precipitates in Nimonic alloy by ultrasonic velocity measurements. Mater Charact 60:234–239
150. Murthy GVS, Das SK, Ravikumar B (2014) Comprehensive microstructural characterization of γ' in a nimonic alloy using ultrasonic velocity measurements. Metallogr Microstruct Anal. doi:10.1007/s13632-014-0143-7
151. Jayakumar T (1997) Microstructural characterization in metallic materials using ultrasonic and magnetic methods. PhD Thesis, University of Saarland
152. Kumar A, Jayakumar T, Raj B (2000) Ultrasonic spectral analysis for microstructural characterization of austenitic and ferritic steels. Phil Mag A 80:2469–2487
153. Iacoviello F, Casari F, Gialanella S (2005) Effect of "475 °C embrittlement" on duplex stainless steels localized corrosion resistance. Corr Sci 47:909–922
154. Chen TH, Weng KL, Yang JR (2002) The effect of high temperature exposure on the microstructural stability and toughness property in a 2205 duplex stainless steel. Mater Sci Eng A 338:259–270
155. Silva E, Albuquerque VHC, Leite JP, Varela AG, Moura EP, Tavares JMRS (2009) Phase transformation evaluation on a UNS S31803 duplex stainless steel based on nondestructive testing. Mater Sci Eng A 516:126–130
156. Freitas VLA, Normando PG, Albuquerque VHC, Silva E, Silva AA, Tavares JMRS (2011) Nondestructive characterization and evaluation of embrittlement kinetics and elastic constants of duplex stainless steel SAF 2205 for different aging time at 425 °C and 475 °C. J Nondestruct Eval 30:130–136
157. Pohl M, Storz O, Glogowski T (2007) Effect of intermetallic precipitations on the properties of duplex stainless steel. Mater Charact 58:65–71
158. Albuquerque VHC, Silva E, Leite JP, Moura EP, Freitas VLA, Tavares JMRS (2010) Spinodal decomposition mechanism study on the duplex stainless steel UNS S31803 using ultrasonic speed measurement. Mater Des 31:2147–2150
159. Matsubara S, Yokono Y, Nagano Y, Imanaka T, Kawaguchi Y, Mitsuda H, Okano Y (1999) Evaluation of thermal aging of duplex stainless steel by means of sound velocity measurement in the fine region using phase interference technique. In: Proceedings of 7th international conference on nuclear engineering, Japan, pp 19–23
160. Matsubara S, Yokono Y, Imanaka T, Kawaguchi Y, Mitsuda H, Okano Y (1998) Evaluation of thermal ageing in duplex stainless steel by velocity measurements of surface acoustic wave. In: Proceedings of 1st international conference on NDE in relation to structural integrity for nuclear and pressurised components, Netherlands, pp 20–22
161. Tane M, Ichitsubo T, Ogi H, Hirao M (2003) Elastic property of aged duplex stainless steel. Scr Mater 48:229–234
162. Choo WK, Kim HJ, Yoon JC (1997) Microstructure changes in austenitic Fe–30.0 wt% Mn–7.8 wt% Al–1.3 wt% C initiated by spinodal decomposition and its influence on mechanical properties. Acta Mater 45:4877–4885
163. Ruiz A, Ortiz N, Carreon H, Rubio C (2009) Utilization of ultrasonic measurement for determining the variation in microstructure of thermally degraded 2205 duplex stainless steel. J Nondestruct Eval 28:131–139
164. Ruiz A, Ortiz N, Medina A, Kim JK, Jacobs LJ (2013) Application of ultrasonic methods for early detection of thermal damage in 2205 duplex stainless steel. NDT E Int 54:19–26
165. Jhang KY (2009) Nonlinear ultrasonic techniques for nondestructive assessment of micro damage in material: a review. Int J Prec Eng Manuf 10:123–135
166. Xiang Y, Deng M, Xuan FZ, Liu CJ (2011) Experimental study of thermal degradation in ferritic Cr–Ni alloy steel plates using nonlinear Lamb waves. NDT E Int 44:768–774
167. Hurley DC, Balzar D, Purtscher PT (2000) Nonlinear ultrasonic assessment of precipitation hardening in ASTM A710 steel. J Mater Res 15:2036–2042
168. Abd Rashid MW, Gakim M, Rosli ZM, Azam MA (2012) Formation of $Cr_{23}C_6$ during the sensitization of AISI 304 stainless steel and its effect to pitting corrosion. Int J Electrochem Sci 7:9465–9477
169. Amuda MOH, Mridha S (2011) An overview of sensitization dynamics in ferritic stainless steel welds. Int J Corros. doi:10.1155/2011/305793
170. Stella J, Cerezo J, Rodriguez E (2009) Characterization of the sensitization degree in the AISI 304 stainless steel using spectral analysis and conventional ultrasonic techniques. NDT E Int 42:267–274
171. Li F, Xiang D, Qin Y, Pond RB Jr, Slusarski K (2011) Measurements of degree of sensitization (DOS) in aluminum alloys using EMAT ultrasound. Ultrasonics 51:561–570